Macro- and Microscopic Fluid Transport in Living Tissues: Application to Solid Tumors

Paolo A. Netti, Laurence T. Baxter, and Yves Boucher
Dept. of Radiation Oncology, Massachusetts General Hospital and Harvard Medical School, Boston, MA 02114

Richard Skalak
Dept. of Bioengineering, University of California, San Diego, CA 92093

Rakesh K. Jain
Steele Lab., Massachusetts General Hospital, Boston, MA 02114

Transvascular and interstitial fluid movements are involved in many important biological processes such as convective macromolecular transport and contribute to the mechanical behavior of tissue. Although intimately coupled, there is a tendency in the literature to regard these two fluid-transport mechanisms separately; if the interaction is considered, the description is usually confined to the local level (e.g., transvascular or interstitial perivascular). A general framework presented here combines transvascular and interstitial fluid movement with the mechanics of soft tissue and integrates macro- and microscopic views of the phenomena. On the macroscopic level, interstitial fluid transport is described by adapting the field equations of the poroelastic theory using average field variables defined on a scale of several blood vessel diameters ($\approx$ 1 mm), while transvascular transport is described by a generalized Starling's law. As an example, the model equations have been specialized for a spherical solid tumor and an analytical solution is presented for the transient redistribution of interstitial fluid following a rapid change in vascular pressure or flow. The model describes the overall average profiles of the interstitial fluid pressure and velocity, as well as the dilatation, displacement and stress of the solid matrix. Moreover, on a smaller length scale the model can describe the local fluid movement (perivascular) using the average field variables as boundary conditions. The basic theory provides new insight into understanding the fluid transport in biological tissues and a valuable tool for determining relevant fluid-transport parameters. Implications for improving drug delivery to solid tumors are also discussed.

Introduction

Convective transport in the gel-like region between cells (interstitium) is important for delivery of drugs and nutrients. To evaluate the phenomena involved, an appropriate description of fluid dynamics through the interstitium is essential. Two continuum models are commonly adapted to describe the mechanics of soft tissue: poroelasticity and mixture theory. The former considers soft tissue to be a fluid-saturated poroelastic solid (a spongelike material) and the latter simulates soft tissue as an intimate mixture of solid and fluid phases (a concentrated macromolecular solution). The poroelastic theory was originally formulated by Biot for the analysis of wet-soil consolidation (1941, 1955), and then applied to soft tissue mechanics (Simon et al., 1983). The mixture theory as developed by Truesdell and Toupin (1960), Bowen (1976, 1980), and others was applied to soft tissue mechanics by Mow et al. (1980) using a linear biphasic model. Although their derivations are slightly different, the two models are equivalent when applied to biomechanical studies (Simon, 1992). Both models describe interstitial fluid movement and the corresponding tissue dilation as pseudodiffusive processes con-

trolled by the tissue hydraulic conductivity and its elastic modulus. The linear biphasic and poroelastic models have been extended to include nonlinearities corresponding to strain-dependent permeability (Holmes et al., 1985; Lai and Mow, 1980), finite deformation (Holmes, 1986; Mow et al., 1986; Simon and Gaballa, 1988a,b), and viscoelasticity (Mak, 1986). These models were developed with the primary aim of describing the load-bearing behavior of soft tissue and applied successfully to articular cartilage (Mow and Lai, 1979; Spilker and Suh, 1990; Spilker et al., 1992), intervertebral discs (Simon and Gaballa, 1988b; Simon et al., 1983), artery walls (Jain and Jayaraman, 1987; Keynton, 1976; Simon and Gaballa, 1988a), and brain tissue (Basser, 1992; Nagashima et al., 1987, 1990), as well as hydrogels (Barocas et al., 1995; Grimshaw et al., 1989). Our interest, however, is focused on the description of the fluid transport processes that occur in these tissues and its relevance to macromolecular transport.

Both the "mixture" and "poroelastic" concepts are continuum approximations of the actual structure of soft tissue that includes fiber matrix, proteins, and fluid. These theories describe fluid movement and other field variables (e.g., solid stress and dilatation) as average quantities over a scale of several pore diameters. On a larger scale (≈ 1 mm), however, tissue is composed not only of this interstitial matrix, but of cells and the microvascular and lymphatic networks. Fluid and solutes are continually exchanged between vascular, interstitial matrix and lymph compartments. An exact analysis of such transport processes would require not only accurate descriptions of the vasculature topology, but also microcirculatory fluid dynamics and cell distribution throughout the tissue as well as their complex interactions. By appropriately defined average variables, however, a more feasible macroscopic approach of the phenomena is possible. In this sense, the interstitial matrix properties are regarded as averages over several cell diameters. The macroscopic fluid movement is described by considering the whole tissue as a continuum and all fluid movement *passive*, that is, driven by hydrostatic and osmotic pressure gradients (Fung, 1990). The entire tissue is described as a fluid-saturated poroelastic medium containing a uniform distribution of fluid source/sink points representing the transvascular flow to or from the interstitial compartment.

The motivation of this work arises mainly from an interest in fluid and macromolecular transport in solid tumors, where the presence of physiological transport barriers can strongly abate the efficiency of therapeutic agents (Jain, 1996a,b). For example, it has been shown that (a) interstitial fluid pressure (IFP) is uniformly elevated throughout a solid tumor and drops precipitously in the tumor periphery (Boucher et al., 1990; Jain and Baxter, 1988), and (b) microvascular pressure is very close to the central IFP (Boucher and Jain, 1992). As a result, the convective component of macromolecular transport across the vessel wall is hindered throughout most of the tumor (Jain, 1987a). To enhance convection, the transmural pressure gradient must be increased, and this could be achieved in principle by elevating vascular pressure (Netti et al., 1995; Zlotecki et al., 1993, 1995). The understanding of fluid transport in tumors and identification of the relevant parameters that control it are therefore crucial for improving the effectiveness of systemic cancer therapies. Along these lines we have previously developed a macroscopic fluid transport model based on a rigid porous material able to describe the steady-state interstitial fluid pressure and velocity profiles (Baxter and Jain, 1989), and more recently we have experimentally tested the validity of the poroelastic model to describe the transient phenomena (Netti et al., 1995).

In this article we have adapted the field equations of the poroelastic model using average field variables defined over the whole tissue and developed a macroscopic continuum model to describe fluid movement within soft tissue. In addition, a local analysis of fluid movement around a single blood vessel has been considered using the average field variables as boundary conditions, providing an integrated macroscopic and microscopic view of fluid transport in tissue.

An analytical solution for a spherical solid tumor and the implication for drug delivery will be discussed. The basic theory presented here may also be of interest to describe fluid-transport phenomena in other pathologies such as edema, ischemia, and local fluid (drug) infusion.

Mathematical Model

Macroscopic analysis

Most tissues or organs of a mammalian body can be subdivided into three compartments: vascular, cellular, and interstitial-lymphatic (Fung, 1990). The relative amount of each phase varies from organ to organ as well as within the same organ. The vascular space is typically a small percentage of the total volume. Capillary diameters generally span from 5 to 20 μm (Fung, 1990), and the typical intercapillary distance is of the order of 100 μm. The space between blood vessels is occupied by the interstitial matrix, which connects the vessel wall to the membrane of cells and is predominantly composed of collagen and elastin fibers. Dispersed within this network are macromolecular constituents (hyaluronate and proteoglycans) and water that form a hydrophilic gel (Fung, 1990; Mow et al., 1980). We will consider the ensemble of interstitial, vascular and cellular spaces as a continuous, deformable solid phase saturated with a fluid phase consisting of water and macromolecular constituents. In this model, only the interstitial fluid is regarded as free to flow: cellular volumes are assumed to be constant. To allow a continuum view, we define as the elementary volume a piece of tissue large enough to contain a sufficiently large number of cells and blood vessels (Figures 1a and 1b), that is, the dimension of the elementary volume is at least one order of magnitude more than the distance between the vessels (> 100 μm). Each of the field variables and parameters that we shall use represents an average quantity defined over the elementary volume:

$$\langle \chi \rangle = \frac{\int_{\delta\Gamma} \chi \, d\Gamma}{\delta\Gamma}, \tag{1}$$

where χ is a generic variable or parameter, and $\delta\Gamma$ is the elementary volume. To distinguish between average and local variables, hereafter we will indicate average variables in boldface and marked with a tilde ($\tilde{}$).

Governing equations

Let $\tilde{\underline{v}}(r,t)$ and $\tilde{\underline{u}}(r,t)$ be the macroscopic fluid velocity and the solid displacement vectors, respectively, and $\tilde{\phi}$ the vol-

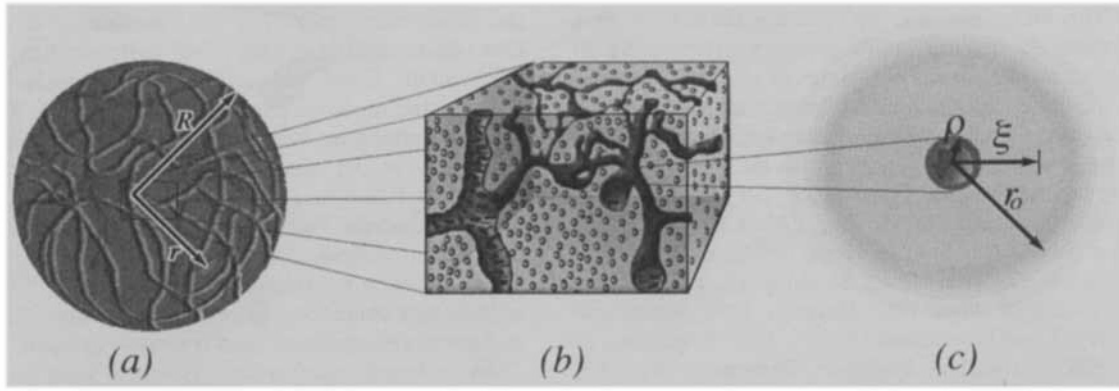

Figure 1. A soft tissue.

At macroscopic level, the tissue is composed of vascular, interstitial, and cellular spaces. In our macroscopic model, we define as the elementary volume a piece of tissue large enough to contain a sufficiently large number of cells and blood vessels (b). The macroscopic field variables and parameters, indicated in the text in boldface and marked with a tilde (~), are defined as an average over this elementary volume; r is the spatial coordinate and R is the macroscopic size. At the microscopic level (i.e., perivascular), the tissue can be described as the interstitial and cellular spaces around a blood vessel (c); ρ is the vessel's diameter; r_o is the penetration depth, defined as that distance from the blood vessel at which the local variables approach the mean field value; ξ is the spatial coordinate.

ume fluid fraction. We assume that the fluid and the solid phases have the same specific volume, that is,

$$\frac{\tilde{\rho}_s}{1-\tilde{\phi}} = \frac{\tilde{\rho}_f}{\tilde{\phi}}.$$

where $\tilde{\rho}_s$ and $\tilde{\rho}_f$ are the mass density of solid and fluid, respectively.

From conservation of mass it follows that

$$\frac{\partial \tilde{\phi}}{\partial t} = -\nabla\cdot\left(\tilde{\phi}\underline{\tilde{v}}\right) + \Omega(\underline{r},t)$$

$$\frac{\partial \tilde{\phi}}{\partial t} = \nabla\cdot\left((1-\tilde{\phi})\frac{\partial \underline{\tilde{u}}}{\partial t}\right), \tag{2}$$

where $\Omega(\boldsymbol{r},t)$ is the fluid source term assumed to be driven by the average transmural pressure:

$$\Omega(\boldsymbol{r},t) = \tilde{\varphi}_V - \tilde{\varphi}_L = \frac{\tilde{L}_p S}{V}(\tilde{p}_v - \tilde{p}) - \frac{\tilde{L}_{pL} S_L}{V}(\tilde{p} - \tilde{p}_L) \tag{3}$$

$\tilde{\varphi}_V$ and $\tilde{\varphi}_L$ represent the transcapillary flow and the lymphatic drainage, respectively; $\tilde{L}_p$ and $\tilde{L}_{pL}$ are the average hydraulic conductivity coefficients of the capillary and the lymphatic walls; S/V and S_L/V are the vascular and lymphatic surface densities in the tumor tissue (vessel surface area (S) per unit of tissue volume (V)); $\tilde{p}_v = \tilde{p}_c - \sigma(\tilde{\pi}_c - \tilde{\pi}_i)$ is the effective vascular pressure; $\tilde{p}_c$ and $\tilde{p}_L$ are the average vascular and lymphatic pressures; and $\tilde{p}$ is the average IFP. The parameters $\tilde{\sigma}$, $\tilde{\pi}_c$, and $\tilde{\pi}_i$ are, respectively, the average osmotic reflection coefficient of plasma proteins, the colloid osmotic pressure of plasma, and the colloid osmotic pressure of interstitial fluid.

By subtracting Eqs. 2, we derive the continuity equation for the mixture:

$$\nabla\cdot\left[\tilde{\phi}\tilde{v} + (1-\tilde{\phi})\frac{\partial \underline{\tilde{u}}}{\partial t}\right] = \Omega(\underline{r},t). \tag{4}$$

The relative movement between the fluid and solid phases is described by the generalized form of Darcy's law:

$$\tilde{\phi}\left(\tilde{v} - \frac{\partial \underline{\tilde{u}}}{\partial t}\right) = -\tilde{K}\nabla\tilde{p}, \tag{5}$$

where $\tilde{K}$ is the average tissue hydraulic conductivity.

The momentum balance for the tissue under the hypothesis of negligible inertial and body forces is

$$\nabla\cdot\underline{\underline{\tilde{\tau}}} = \underline{\underline{0}}, \tag{6}$$

where $\underline{\underline{\tilde{\tau}}}$ represents the effective tissue stress tensor. Assuming the solid matrix to behave as a linear elastic material in the limit of small strain, the average velocity field is irrotational, and the constitutive equation for the tissue is

$$\underline{\underline{\tilde{\tau}}} = -\tilde{p}\underline{\underline{I}} + \tilde{\lambda}\tilde{e}\underline{\underline{I}} + 2\tilde{\mu}\underline{\underline{\tilde{\varepsilon}}}, \tag{7}$$

where $\tilde{\mu}$ and $\tilde{\lambda}$ are the Lamé constants of the elastic solid matrix. The matrix dilatation, $\tilde{e}$, is the divergence of the solid displacement vector:

$$\tilde{e} = \mathrm{Tr}\left(\underline{\underline{\tilde{\varepsilon}}}\right) = \nabla\cdot\underline{\tilde{u}}. \tag{8}$$

The infinitesimal network strain tensor $\underline{\underline{\tilde{\varepsilon}}}$, is

$$\underline{\underline{\tilde{\varepsilon}}} = \frac{1}{2}(\nabla\underline{\tilde{u}} + \nabla\underline{\tilde{u}}^T). \tag{9}$$

The hypothesis of linear elasticity and small strain is not as limiting as it would first appear. In biomechanical studies, the poroelastic or biphastic models have been extended with

finite deformation and nonlinear elasticity to solve canonical problems of soft tissue mechanics (Mow et al., 1986; Simon, 1992; Spilker and Suh, 1990; Spilker et al., 1992), demonstrating the importance of the fluid pressurization in the load support mechanisms of these tissues. The objective of our study, however, is to describe the fluid transport mechanisms occurring throughout the tissue rather than the stress distribution and load-bearing behavior of soft tissue. The IFP field in this case does not arise from an external load, but is generated by an unbalanced extravasation of vascular fluid in the interstitium and does not exceed the order of 10 mm Hg. The hypothesis of linear elasticity and small strain is thus legitimate for these low stress levels.

It is worthwhile noting here that Eq. 7 does not imply that the fluid phase is inviscid. Equation 5 implies that the relative velocity field (i.e., $\underline{\tilde{v}} - (\partial \underline{\tilde{u}}/\partial t)$) is irrotational. Furthermore, from the hypothesis of elasticity of the solid phase, it follows that the solid-velocity and fluid-velocity fields are both irrotational. The average fluid-velocity field is thus irrotational and contributes only the hydrostatic pressure in Eq. 7.

From Eqs. 6 and 7, we have

$$\tilde{\mu}\nabla^2\underline{\tilde{u}} + \left(\tilde{\mu} + \tilde{\lambda}\right)\nabla(\nabla\cdot\underline{\tilde{u}}) - \nabla\tilde{p} = 0. \tag{10}$$

The divergence of this yields

$$(2\tilde{\mu} + \tilde{\lambda})\nabla^2\tilde{e} = \nabla^2\tilde{p}. \tag{11}$$

From Eqs. 4 and 5, we have the result:

$$\nabla\cdot\left(-\tilde{K}\nabla\tilde{p} + \frac{\partial\underline{\tilde{u}}}{\partial t}\right) = \Omega(\underline{r}, t). \tag{12}$$

Assuming $\tilde{K}$ to be independent of the tissue deformation:

$$\frac{\partial\tilde{e}}{\partial t} - \tilde{K}\nabla^2\tilde{p} = \Omega(\underline{r}, t). \tag{13}$$

Finally, substituting Eq. 11 into Eq. 13, we obtain

$$\frac{\partial\tilde{e}}{\partial t} - \tilde{K}(2\tilde{\mu} + \tilde{\lambda})\nabla^2\tilde{e} = \Omega(\underline{r}, t). \tag{14}$$

The lefthand side (LHS) of Eq. 14 is the usual expression derived from the poroelastic or mixture theory and, when set equal to zero, describes the transient evolution of the tissue dilatation due to fluid percolation through the tissue. The righthand side (RHS) is a new term introduced here to account for the transcapillary fluid exchange. Mathematically, Eq. 14 is similar to a diffusion equation with a chemical reaction: the product $\tilde{K}(2\tilde{\mu} + \tilde{\lambda})$ represents a *pseudo*diffusion coefficient and $(\tilde{L}_p S/V - \tilde{L}_{pL} S_L/V)$ represents a *pseudo*-first-order reaction constant. Therefore, by analogy to the diffusion-reaction process, we can conclude that transient interstitial fluid redistribution in a tissue may occur via two distinct pathways: a percolation mechanism through the interstitium and a transcapillary fluid exchange.

The tissue fluid volume fraction $\tilde{\phi}$ is a function of the dilatation; for small deformation the dilatation may be written as follows:

$$\tilde{e} = \frac{\delta V_t}{V_t^o} \approx \frac{V_t - V_t^o}{V_t^o}, \tag{15}$$

where V_t and V_t^o are the volumes of a deformed and undeformed tissue element. Fluid enters or leaves the tissue element, but the variations of the fluid volume (δV_f) and tissue volume (δV_t) volume are equal and opposite:

$$V_t^0\tilde{\phi}^o - V_t\tilde{\phi} = V_t^o - V_t \tag{16}$$

where $\tilde{\phi}^o$ is the fluid volume fraction of the undeformed tissue. From Eqs. 15 and 16, we have:

$$\tilde{\phi} = \frac{\tilde{e} + \tilde{\phi}^o}{1 + \tilde{e}}. \tag{17}$$

In the following subsection we will give an example of the macroscopic model applied to the description of fluid transport in a spherical solid tumor.

Solid Tumors. Like every tissue or organ, a tumor is composed of vascular, interstitial, and cellular spaces, but there are significant differences in structure, composition, and physiology between normal and neoplastic tissues (Jain, 1987a,b, 1994; Jain et al., 1980). Experimental evidence suggests that most tumors lack an anatomically well-defined lymphatic network (Gullino, 1975). Also, cellular growth and remodeling are particularly active within a tumor and may lead to spatial and temporal heterogeneities in cellular and vascular densities. However, because the time scale of the fluid transport phenomena is much smaller than the characteristic time scale of growth and remodeling, any temporal heterogeneity within the tumor tissue can be neglected in the present context. Furthermore, while the spatial heterogeneity is crucial in determining the microscopic behavior of the system, its effect can be averaged out over a macroscopic scale (Baxter and Jain, 1989).

In the case of a spherical, homogeneous tumor (Figure 1a), the field equations can be rewritten as follows: the momentum balance (Eq. 6):

$$(2\tilde{\mu} + \tilde{\lambda})\frac{\partial\tilde{e}}{\partial r} = \frac{\partial\tilde{p}}{\partial r}; \tag{18}$$

the conservation equation (Eq. 14):

$$\frac{\partial\tilde{e}}{\partial t} - \tilde{K}(2\tilde{\mu} + \tilde{\lambda})\frac{1}{r^2}\frac{\partial}{\partial r}\left(r^2\frac{\partial\tilde{e}}{\partial r}\right) = \Omega(r, t). \tag{19}$$

Assuming that lymphatic drainage is negligible, the fluid generation term (Eq. 3) can be rewritten as

$$\Omega(r, t) = \tilde{\varphi}_V = \frac{\tilde{L}_p S}{V}(\tilde{p}_v - \tilde{p}). \tag{20}$$

For simplicity, we will consider only the case of an isolated tumor, that is, a tumor that is not surrounded by normal tissue. The extension to a nonisolated tumor that interacts with

the surrounding tissue would require changes in the outer boundary conditions.

On the surface of an isolated tumor of radius R there are no contact forces, and so the fluid pressure and normal solid stresses are zero:

$$\begin{cases} \tilde{p} = 0 & \text{at} \quad r = R \qquad (21) \\ \tilde{\tau}_{rr} = 2\tilde{\mu}\dfrac{\partial \tilde{u}_r}{\partial r} + \tilde{\lambda}\tilde{e} = 0 & \text{at} \quad r = R, \qquad (22) \end{cases}$$

where $\tilde{u}_r$ is the radial displacement of the tissue. Equation 22 can be rewritten as

$$\tilde{e} = 4\frac{\tilde{\mu}}{2\tilde{\mu} + \tilde{\lambda}}\frac{\tilde{u}_r}{R} \quad \text{on} \quad r = R. \qquad (23)$$

Under the hypothesis of small deformation with tumor radius of $O(1$ cm), the ratio $\tilde{u}_r/R|_R \ll 1$. Furthermore, it has been reported that $\tilde{\mu} \ll \tilde{\lambda}$ for both living soft tissue and synthetic hydrogels (Nagashima et al., 1987; Tanaka and Fillmore, 1978), so that as a first approximation one can assume $\tilde{e}(r = R, t) \to 0$.

To solve Eq. 19 it is necessary to know the functional relationship between IFP (which occurs in Ω) and tissue dilatation. This can be obtained by solving Eq. 18, using as a boundary condition $\tilde{e}(\tilde{p} = 0) = 0$:

$$\tilde{e} = \frac{\tilde{p}}{(2\tilde{\mu} + \tilde{\lambda})}. \qquad (24)$$

Combining Eqs. 19 and 24 and introducing dimensionless radius $\hat{r}$ and time, $\hat{t}$:

$$\frac{\partial \tilde{e}}{\partial \hat{t}} - \frac{1}{\hat{r}^2}\frac{\partial}{\partial \hat{r}}\left(\hat{r}^2\frac{\partial \tilde{e}}{\partial \hat{r}}\right) + \tilde{\alpha}^2\tilde{e} = \frac{\tilde{\alpha}^2}{(2\tilde{\mu} + \tilde{\lambda})}\tilde{p}_v, \qquad (25)$$

where $\hat{t} = t/(R^2/\tilde{K}(2\tilde{\mu} + \tilde{\lambda}))$ and $\hat{r} = r/R$. The dimensionless parameter

$$\tilde{\alpha} = R\sqrt{\frac{\tilde{L}_p S}{\tilde{K} V}}$$

controls the physical phenomena of the fluid movement; it is the equivalent of the Damkohler number in that it represents the ratio between the resistance to interstitial percolation and the resistance to transcapillary fluid exchange.

The boundary conditions are

$$\begin{cases} \tilde{e} = 0 & \text{at} \quad \hat{r} = 1 \\ \dfrac{\partial \tilde{e}}{\partial \hat{r}} = 0 & \text{at} \quad \hat{r} = 0. \end{cases} \qquad (26)$$

The initial conditions must be derived from the steady-state pressure and velocity profiles.

In the following subsections, Eq. 25 will be solved for both the steady state and the transient evolution following changes in either vascular pressure or vascular flow.

Steady State. In the steady state, Eq. 25 becomes:

$$\frac{\partial^2 \tilde{e}}{\partial \hat{r}^2} + \frac{2}{\hat{r}}\frac{\partial \tilde{e}}{\partial \hat{r}} - \tilde{\alpha}^2\tilde{e} = -\frac{\tilde{\alpha}^2}{(2\tilde{\mu} + \tilde{\lambda})}\tilde{p}_o \qquad (27)$$

where $\tilde{p}_o$ is the average steady state microvascular pressure. Equation (27), a modified Helmholtz equation, can be integrated using spherical Bessel functions to obtain:

$$\tilde{e}(\hat{r}) = \frac{\tilde{p}_o}{(2\tilde{\mu} + \tilde{\lambda})}\left(1 - \frac{\sinh(\tilde{\alpha}\hat{r})}{\hat{r}\sinh(\tilde{\alpha})}\right) \qquad (28)$$

from Eq. 24:

$$\tilde{p}(\hat{r}) = \tilde{p}_o\left(1 - \frac{\sinh(\tilde{\alpha}\hat{r})}{\hat{r}\sinh(\tilde{\alpha})}\right) \qquad (29)$$

The macroscopic fluid velocity can be obtained by Darcy's law (Eq. 5):

$$\tilde{v}_r(\hat{r}) = \frac{\tilde{K}\tilde{p}_0}{R\tilde{\phi}}\left(\frac{\tilde{\alpha}\hat{r}\cosh(\tilde{\alpha}\hat{r}) - \sinh(\tilde{\alpha}\hat{r})}{\hat{r}^2\sinh(\tilde{\alpha})}\right) \qquad (30)$$

Transient Process. Physiologically, fluid redistribution throughout the tumor interstitium may occur as a consequence of a change in either microvascular pressure or vascular flow. In the Appendix the analytical solutions of the model for these two cases are derived.

Microscopic analysis

The macroscopic field variables (e.g., fluid velocity and interstitial pressure) arise from an integrated view of the tissue and do not describe local phenomena that occur around a single blood vessel. We now describe perivascular fluid flow by regarding the capillary as a rigid cylinder (Krogh cylinder (Krogh, 1922)) with a uniform diameter of 15 μm (Jain, 1988) embedded in a poroelastic medium (the interstitial matrix (Figure 1c). Further assumptions are noninteraction of neighboring vessels; absence of axial pressure gradients; and constant hydraulic permeabilities of both the vessel wall (L_p) and interstitial matrix (K). Although the Krogh cylinder model has been used for more detailed analyses of perivascular transport (for example, to include axial pressure gradients (Apelblat et al., 1974), or incorporate the effects of variable vessel diameter, vascular permeability, tissue conductivity, and porosity (An and Salathe, 1976; Salathe and An, 1976), these approaches are limited to the local scale without considering their effects on the macroscale. The novelty of our approach is that the average field variables are used as boundary conditions, enabling the integration of macroscopic and microscopic analyses.

Governing equations

Looking at a microscopic scale, the "fluid generation term" moves from the domain to the boundary. For the interstitial matrix surrounding the blood vessel, we rewrite Eq. 11, setting the generation term to zero:

$$\frac{\partial e}{\partial t} - K(2\mu + \lambda)\frac{1}{\zeta}\frac{\partial}{\partial \zeta}\left(\zeta \frac{\partial e}{\partial \zeta}\right) = 0. \tag{31}$$

Here all the variables and parameters are local in that they refer to the interstitial matrix and not to the whole tissue. The spatial coordinate is indicated by ξ. In the case of axial symmetry, the momentum balance (Eq. 10) becomes

$$(2\mu + \lambda)\frac{\partial e}{\partial \zeta} = \frac{\partial p}{\partial \zeta}. \tag{32}$$

Steady State. In the steady state, Eqs. 31 and 32 are combined to yield

$$\frac{\partial}{\partial \zeta}\left(\zeta \frac{\partial p}{\partial \zeta}\right) = 0, \tag{33}$$

with boundary conditions

$$\begin{cases} p = \tilde{p} & \text{at} \quad \zeta = r_o \\ -K\dfrac{\partial p}{\partial \zeta} = L_p(p_v - p) & \text{at} \quad \zeta = \rho, \end{cases} \tag{34}$$

where p_v is the vascular pressure of the particular vessel, ρ is its radius, and r_o is the penetration depth defined as the distance from the blood vessel at which the local pressure approaches the mean field value. The first boundary condition assumes, subject to *a posteriori* verification, that there are no interactions between neighboring vessels (i.e., r_o is less than half the distance between vessels).

The solution of Eqs. 33 and 34 is

$$p = \frac{\alpha_L}{1 + \alpha_L \ln(r_o/\rho)}(p_v - \tilde{p})\ln\left(\frac{r_0}{\zeta}\right) + \tilde{p}. \tag{35}$$

From Eq. 35 and Darcy's law, the velocity profile is

$$v = \frac{L_p}{1 + \alpha_L \ln(r_o/\rho)}(p_v - \tilde{p})\frac{\rho}{\zeta}, \tag{36}$$

where $\alpha_L = (L_p \rho/K)$ is the microscopic equivalent of the macroscopic parameter $\tilde{\alpha}$: the local ratio of transvascular to interstitial fluid-flow resistances.

The parameter α_L governs the pressure profile around the blood vessel but not the average IFP. For example, the fluid pressure on the vessel surface is

$$p|_\rho = p_v - \frac{1}{1 + \alpha_L \ln(r_o/\rho)}(p_v - \tilde{p}). \tag{37}$$

When $\alpha_L \gg 1$, the vascular resistance is negligible compared to the interstitial resistance, and therefore the fluid pressure in proximity of the blood vessel will be close to the vascular pressure. On the other hand, when $\alpha_L \ll 1$, this pressure will be close to the average IFP.

It should be noted that for large values of macroscopic $\tilde{\alpha}$, Eq. 30 predicts that in the central area of a solid tumor $\tilde{p} \approx \tilde{p}_o$, which does not necessarily mean that there is no fluid extravasation from blood vessels. This flux across the vessel wall can be evaluated as

$$J_v = \frac{L_p}{1 + \alpha_L \ln(r_0/\rho)}(p_v - \tilde{p}). \tag{38}$$

Fluid can still extravasate or be reabsorbed even if $\tilde{p} \approx \tilde{p}_o$; the complete absence of transcapillary flow would require a strictly uniform vascular pressure (i.e., $p_v = \tilde{p}_o$).

Transient Process. While the capillary wall is a poroelastic material itself (Jain and Jayaraman, 1987), its thickness is much smaller than the vessel diameter, and so the characteristic time for transvascular fluid flow is negligible compared to that of interstitial flow. Therefore, the pressure distribution across the vessel wall can be considered as the quasi steady state that would occur in a rigid porous material. Under this hypothesis, the transvascular fluid flow can be described by the Starling's law (Fung, 1990).

The boundary conditions are:

$$\begin{cases} u_\zeta(\rho, t) = 0 \\ \tau_{\theta\theta}(\rho, t) = -p(\rho, t) + \lambda e(\rho, t) + 2\mu\dfrac{u_\zeta(\rho, t)}{\rho} = 0. \end{cases} \tag{39}$$

From Eqs. 39 and 32 we obtain

$$(2\mu + \lambda)e(r, t) = p(r, t) + \frac{2\mu}{\lambda}p(\rho, t). \tag{40}$$

To solve the transient fluid transport problem it is convenient to rewrite Eq. 31 in terms of variation with respect to the initial steady state [Note: hereafter deviations from the steady state are marked with an asterisk $(*)$, i.e., $p^*(\zeta, t) = p(\zeta, t) - p(\zeta, 0)$]:

$$\frac{\partial p^*}{\partial t} - K(2\mu + \lambda)\frac{1}{\zeta}\frac{\partial}{\partial \zeta}\left(\zeta \frac{\partial p^*}{\partial \zeta}\right) = -\frac{\lambda}{2\mu}\frac{d}{dt}[p(\rho, t)]. \tag{41}$$

In the following section we determine the perivascular fluid redistribution following a rapid change in vascular pressure.

Change in Microvascular Pressure. The initial and boundary conditions will be:

$$\begin{cases} p^*(\zeta, 0) = 0 \\ p^*(r_o, t) = \tilde{p}^*(t) \\ -K\left.\dfrac{\partial p^*}{\partial \zeta}\right|_\rho = L_p(p_v^* - p^*(\rho, t)). \end{cases} \tag{42}$$

Equations 41 and 42 have been solved numerically by spatial discretization, approximating the partial differential equation as a system of 40 ordinary differential equations solved with a Runge-Kutta method of the fifth order.

Table 1. Physiological Transport Parameters

Parameter	Value	Reference
$\tilde{L}_p$	3.6×10^{-7} cm/mm Hg·s	Baxter and Jain (1989)
$\tilde{K}$	4.13×10^{-8} cm^2/mm Hg·s	Swabb et al. (1974)
S/V	200 cm^{-1}	Hilmas and Gilette (1974)
$\tilde{\lambda}$	684 mm Hg	Nicholson and Phillips (1981)
$\tilde{\mu}$	15.2 mm Hg	Nicholson and Phillips (1981)
$\tilde{\phi}$	0.2	Jain (1987b)

Only the values of $\tilde{K}$ and S/V are evaluated for tumor tissues; all the other parameters pertain to other tissue and have been adapted to tumor (see Netti et al., 1995).

Parameter values

To simulate the transient fluid redistribution described by the model, values for the physiological fluid transport and mechanical parameters of solid tumors are needed. Table 1 shows the parameters used for the simulations. Because they have been evaluated experimentally, each of these parameters refers to the macroscopic value. Due to original heterogeneity within the tissue, significant variations at the local level are likely.

Results

Macroscopic analysis

The spatial and temporal evolutions of average IFP and fluid velocity were calculated by using a minimum of 400 terms in the series representing the analytical solution. The actual number of terms used was established by terminating at a relative error of 10^{-5}.

Steady State. The steady-state interstitial fluid pressure and velocity profiles are described by Eqs. 29 and 30. IFP profile is controlled by $\tilde{\alpha}$: for low value of $\tilde{\alpha}$, IFP is close to zero, for high value of $\tilde{\alpha}$, IFP is uniformly elevated throughout the tumor and drops abruptly in the periphery.

Transient Process. Central Interstitial Fluid Pressure. The effect of the parameter $\tilde{\alpha}$ on the transient evolution of the IFP in the center of a solid tumor is shown in Figure 2. The difference $(\tilde{p}-\tilde{p}_o)/(x-1)$ is plotted against dimensionless time

$$\left(\hat{t}=\frac{t}{R^2/\tilde{K}(2\tilde{\mu}+\tilde{\lambda})}\right).$$

The solid lines show the results of simulations for a rapid change in the average vascular pressure ($x=(\tilde{p}_v^{fin}/\tilde{p}_o)>1$ represents a pressure increase and $x<1$ represents a pressure decrease). The dotted lines indicate solutions for a rapid decrease of the vascular flow to zero (in this case x has been set to zero). Following a rapid change in vascular pressure, the IFP presents a positive curvature, and the time required to reach the final steady state decreases with $\tilde{\alpha}$. Conversely, the evolution of IFP following a cessation of vascular flow is characterized by a sigmoidal shape that becomes more pronounced at higher value of $\tilde{\alpha}$. In this case the characteristic transient time does not change with $\tilde{\alpha}$. Note that when $\tilde{\alpha}^2/\pi^2<1$ the evolution for a rapid change in vascular pressure and a rapid decrease in vascular flow tend to coincide. Furthermore, since the parameter $\tilde{\alpha}$ controls IFP in the steady state (Eq. 29), for $\tilde{\alpha}^2/\pi^2<1$ the average interstitial fluid pressure is essentially zero everywhere in the tissue and would not be affected by any change in vascular pressure.

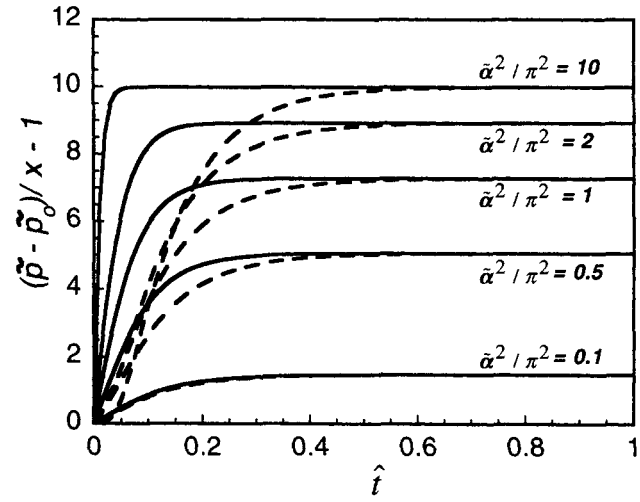

Figure 2. Transient evolution of the IFP in a solid tumor following a rapid change in vascular pressure (——) and a rapid cessation of vascular flow (----).

The characteristic transient time decreases with the ratio $\tilde{\alpha}^2/\pi^2$. For $\tilde{\alpha}^2/\pi^2>1$ the transient process following a rapid change in vascular pressure occurs via a transvascular fluid exchange, which is much faster than the fluid percolation process that occurs following a rapid cessation of vascular flow. As $\tilde{\alpha}^2/\pi^2$ decreases, both transient processes occur via a percolation mode, and the curves coincide.

Predictions using physiological parameters

Predictions of the evolution of the fluid pressure and velocity profiles obtained using the parameters of Table 1 are shown in Figures 2, 3 and 4. The average IFP and velocity are shown as functions of the dimensionless distance from the tumor center at various times.

Abrupt Change of Vascular Pressure. Figure 3A shows the evolution of the IFP profile in a solid tumor when the average vascular pressure is lowered from 10 to 3 mmHg. The IFP decays gradually throughout the tumor. The constancy of pressure in the central region of the tumor during the transient state indicates an absence of macroscopic interstitial fluid flow. In the periphery, the pressure profile drops sharply, but the fluid flow is inwardly oriented (Figure 3B). This intriguing behavior is a consequence of the fluid reabsorption introduced as a generation term in the field equations. Confusion may arise in observing that the velocity has the same direction as the pressure gradient. The apparent paradox stems from the poroelastic nature of the medium considered. The material is deformable and the pressure gradient acts on the *relative* velocity between solid and fluid phase (Eq. 4). The relative fluid velocity always follows the pressure gradient, but fluid and solid velocities do not. In particular, during shrinkage of the solid phase, the resultant fluid velocity may have the same direction as the pressure gradient.

Note that the relative velocity profile, which represents the net fluid flux and determines the convective contribution of transport of macromolecules, can be obtained as the slope of the pressure profile shown in Figure 3A.

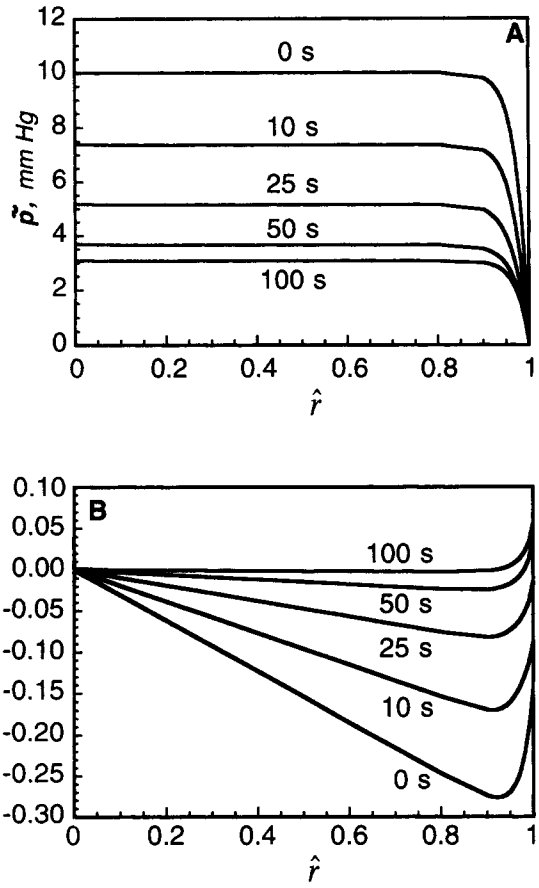

Figure 3. Transient evolution of IFP (A) and velocity (B) in a solid tumor following a rapid decrease of the vascular pressure from 10 to 3 mm Hg.

The value of the parameter $\tilde{\alpha}$ used for this simulation is 40 according to the physiological parameters of Table 1. Note that the pressure profile in the tumor center is always flat, indicating that the transient evolution occurs via a transvascular fluid exchange (A). As a consequence of the transvascular fluid reabsorption, the velocity changes direction transiently, becoming inwardly oriented.

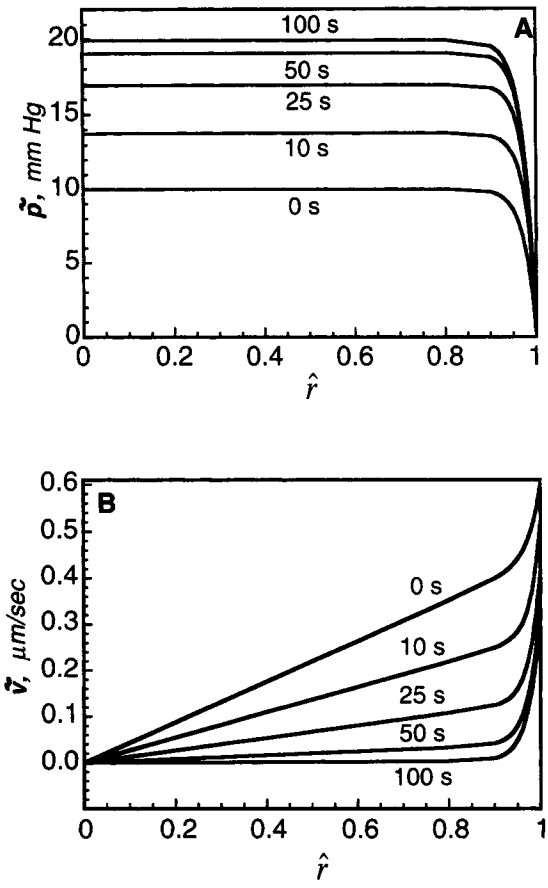

Figure 4. Transient evolution of IFP (A) and velocity (B) in a solid tumor following a rapid doubling of the vascular pressure from 10 to 20 mm Hg.

The value of the parameter $\tilde{\alpha}$ used for this simulation is 40 according to the physiological parameters of Table 1. Fluid extravasates and accumulates in the interstitial space leading to an increase of the interstitial pressure (A). The fluid extravasation leads to an acceleration of the interstitial fluid toward the tumor periphery (B).

The model predictions of IFP and fluid-velocity profiles for a rapid increase of 10–20-mm Hg in vascular pressure are shown in Figures 4A and 4B, respectively. Again, there is a gradual and uniform approach to the final steady state, that is, the response of the system to an increase or a decrease of vascular pressure is symmetric. The fluid velocity at the tumor periphery in this case does not change direction but remains outwardly oriented.

Abrupt Cessation of Transvascular Flow. In this case IFP is not as spatially uniform as in the previous cases (Figure 5A). During the transient phase, pressure gradients develop throughout the tissue, indicating a net outwardly oriented fluid flow (Figure 5B). The decay evolves over a much longer time scale than in the previous case.

Microscopic analysis

Steady State. The microscopic model permits us to describe the fluid transport in the vicinity of a single blood vessel provided that there are no interactions between neighboring vessels. This means that the perivascular pressure gradient, which according to Eq. 35 depends on α_L, ρ, and p_v, must vanish at a distance from the blood vessel less than the average intercapillary space. At given α_L, ρ, and p_v, the penetration depth r_o represents the distance from the blood vessel at which the perivascular pressure gradient vanishes. From Eq. 35, we have

$$\left.\frac{dp}{d\zeta}\right|_{r_o} = -\frac{\alpha_L}{1+\alpha_L \ln(r_o/\rho)}\frac{(p_v-\tilde{p})}{r_o}. \qquad (43)$$

Figure 6 shows the plot of Eq. 43 for different values of α_L using a vessel diameter of 15 μm and a local vascular pressure (p_v) that is twofold higher than the average vascular pressure ($\tilde{p}_o$). This latter assumption is based on experimental observations that tumor microvascular pressure ranges between 7 and 31 mm Hg, with an average of 17 mm Hg (Boucher and Jain, 1992). For all values of α_L the gradient $dp/d\zeta|_{r_o}$ drops rapidly and approaches zero asymptotically at large distances from the vessel. Note that, for all α_L values considered, most of the drop occurs within a distance of 100

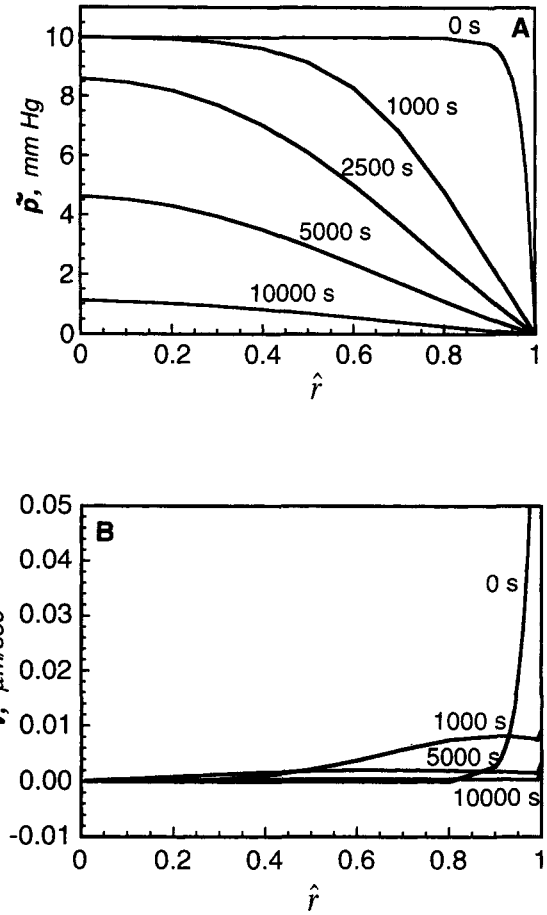

Figure 5. Transient evolution of IFP (A) and velocity (B) in a solid tumor following a rapid cessation of vascular flow.

The value of the parameter $\tilde{\alpha}$ used for this simulation is 40, as evaluated from the physiological parameters of Table 1. During the transient process, interstitial pressure gradients are established in the central region of the tumor that drain fluid toward the periphery (A); accordingly the fluid velocity gradually decreases with time.

μm from the vessel. Therefore, at a distance from blood vessel larger than 100 μm the interstitial fluid pressure is constant and equal to the average $\tilde{p}$. Since the intercapillary distance in tumor tissues is approximately 100 μm, we conclude that the hypothesis of noninteracting vessels is plausible.

Figure 7 shows the influence of the microscopic α_L and macroscopic $\tilde{\alpha}$ parameters on the perivascular pressure profile. The curves have been obtained by plotting Eq. 35 using a vessel diameter of 15 μm and a local vascular pressure (p_v) twofold higher than the average vascular pressure ($\tilde{p}_o$). At fixed value of $\tilde{\alpha}^2$ (i.e., with the same macroscopic interstitial fluid pressure distribution) the perivascular fluid flow increases with α_L, as indicated by the increase in steepness of the pressure profile. Conversely, at fixed α_L, the fluid extravasation decreases with $\tilde{\alpha}^2$. Note that for $\tilde{\alpha}^2 = 100$ (i.e., $\tilde{p} \approx \tilde{p}_o$) the fluid extravasation is strongly reduced as a consequence of an elevated average interstitial pressure.

The fluid flux across the single blood vessel is described by Eq. 38; therefore, the extravasating fluid over a tissue region of volume $\delta\Gamma$ is given by

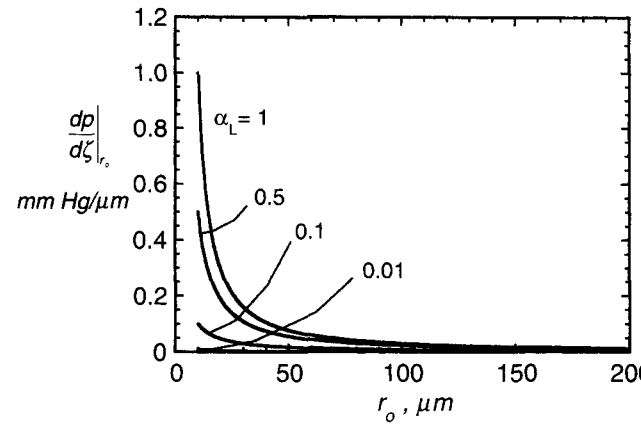

Figure 6. Dependence of the perivascular pressure distribution from the penetration depth for different values of α_L.

$dp/d\zeta|_{r_o}$ represents the perivascular pressure gradient at a distance r_o from the vessel. For all values of the parameter α_L, most of the $dp/d\zeta|_{r_o}$ decay occurs within a distance of 100 μm from the vessel surface. This indicates that if the distance between tumor vessels is larger than 100 μm, the perivascular pressure profiles of two neighboring vessels do not overlap.

$$\tilde{\varphi}_V = \frac{L_p}{1+\alpha_L \ln(r_o/\rho)} \frac{1}{\delta\Gamma} \int_{\delta\Gamma} (p_v - \tilde{p}) \frac{S}{V} d\Gamma$$

$$= \frac{L_p S/V}{1+\alpha_L \ln(r_o/\rho)} (\tilde{p}_o - \tilde{p}). \quad (44)$$

Comparing Eqs. 44 and 3 it is possible to obtain the relationship between the macroscopic and microscopic hydraulic permeabilities of the vessel wall:

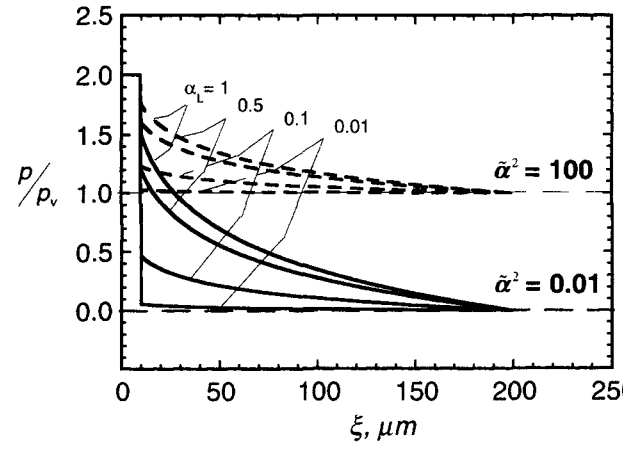

Figure 7. Steady-state perivascular fluid-pressure distribution for different values of local α_L.

The vessel pressure (p_v) is assumed twofold higher than the average vascular pressure $\tilde{p}_v$. At fixed value of $\tilde{\alpha}^2$ (with the same macroscopic interstitial fluid-pressure distribution $\tilde{a}^2 = 0.01$ solid line, $\tilde{a}^2 = 100$ dotted line) the perivascular fluid flow increases with α_L, as indicated by the increase in steepness of the pressure profile. At fixed α_L, the fluid extravasation decreases with $\tilde{\alpha}^2$. Note that for $\tilde{\alpha}^2 = 100$ ($\tilde{p} \approx \tilde{p}_o$) the fluid extravasation is strongly reduced.

$$\tilde{L}_p = \frac{L_p}{1 + \alpha_L \ln(r_o/\rho)}.$$

In the case of $\alpha_L \ll 1$, $\tilde{L}_p \approx L_p$.

Transient Process. The transient analysis was focused on the effects of intercapillary distance and vascular pressure on the perivascular IFP distribution. Figure 8 shows this distribution following an increase of 20 mmHg in vascular pressure. For these simulations we assumed steady-state vascular and interstitial pressures of 20 and 10 mm Hg, respectively, and a local α_L value of 8×10^{-3}. Assuming an intercapillary distance (Δ) of 200 μm, the pressure profile is strictly monotonic, that is, fluid extravasates and accumulates in the interstitium leading to an increase of the average IFP (Figure 8A). For $\Delta = 600$ μm (Figure 8B), the average IFP rises faster than the local pressure, as indicated by the value less than unity of the ratio $p/\tilde{p}$. As a consequence, during the transient fluid redistribution there will be an inversion of the perivascular fluid flow, as indicated by the nonmonotonic behavior of the pressure profile.

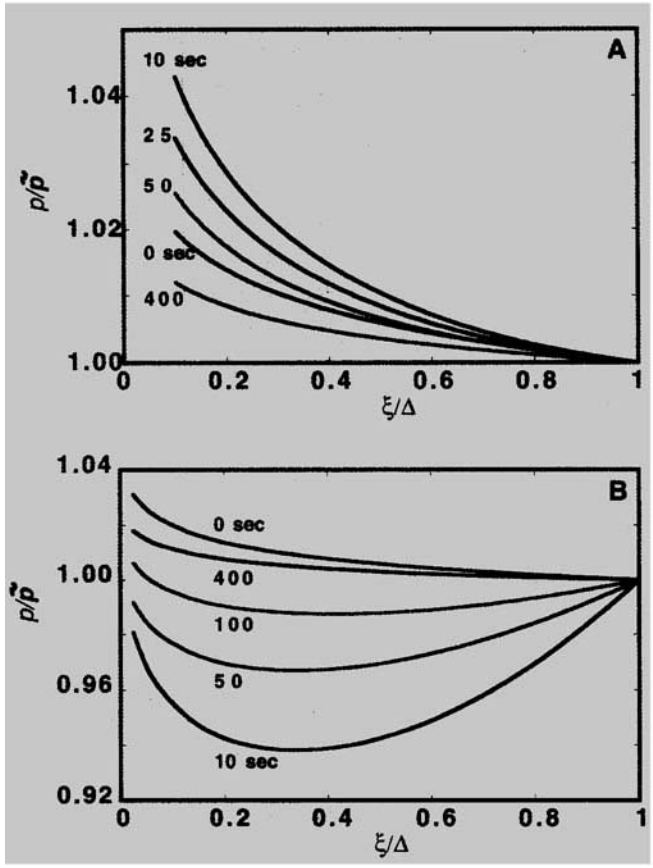

Figure 8. Transient evolution of the perivascular fluid pressure following an increase of 20 mm Hg of vascular pressure.

The value of the parameter ($\tilde{\alpha}$) used for this simulation is 40 according to the physiological parameters of Table 1. For an intercapillary distance of 200 μm (A) the perivascular pressure profile is strictly decreasing and fluid flow extravasates and accumulates in the interstitium. For an intercapillary distance of 600 μm (B), the average IFP is transiently higher than the perivascular pressure and the fluid flow changes direction.

Discussion

Macroscopic analysis

The macroscopic model presented here describes interstitial and transvascular fluid-transport processes as occurring in a spongelike material containing a distribution of fluid source and/or sink points.

Steady State. In the steady state, the interstitial fluid pressure profile is controlled by the ratio of interstitial to transvascular fluid transport resistances: $\tilde{\alpha} = R\sqrt{\left(\tilde{L}_p S/\tilde{K}V\right)}$ (Eq. 29). As an example, consider the IFP in the center of the tumor:

$$\tilde{p}(\hat{r} = 0) = \tilde{p}_o\left(1 - \frac{\tilde{\alpha}}{\sinh(\tilde{\alpha})}\right).$$

If $\tilde{\alpha} \gg 1$, then $\tilde{p} \to \tilde{p}_o$; fluid accumulates in the interstitium and an elevated fluid pressure results. If $\tilde{\alpha} \ll 1$, $\tilde{p} \to 0$ because the small amount of fluid that extravasates is readily filtered out from the interstitium. The former case, however, does not necessarily imply an absence of extravasation in the center of solid tumor (see Eq. 20); rather it indicates that over a dimension of a few vessels, the extravasated fluid balances with that reabsorbed.

Due to the assumption of constant fluid transport parameters, the steady-state solution coincides with that obtained by assuming the interstitial matrix as a rigid porous material (Baxter and Jain, 1989); that is, the parameter $\tilde{\alpha}$ determines the distribution of IFP in a solid tumor. In addition to yielding the rigid porous model results of Baxter and Jain (1989), the present model describes the dilatation and displacement distribution of the tissue and offers the possibility of accounting for the effects of tissue hydration. It should be noted that the fluid velocity used here is the macroscopic fluid velocity normalized to the void fraction of the tissue rather than the Darcy's velocity (which would be $\tilde{\phi}\tilde{v}_r$ in the present notation) used by Baxter and Jain (1989).

Transient Process. When the vascular pressure or flow is changed, both solid and fluid phases undergo transient redistribution. The characteristic time over which these redistributions occur is governed by the fluid-transport parameters and the elasticity of the extracellular matrix. Interstitial and transvascular fluid-transport occur simultaneously, and the dominant pathway is determined by the ratio of their relative resistances $\tilde{\alpha}$. If $\tilde{\alpha} \gg 1$, the interstitial fluid will be preferentially reabsorbed into the capillary network, and if $\tilde{\alpha} \ll 1$, it will preferentially percolate throughout the tissue. We term the former *transvascular mode* and the latter *percolation mode*. The discrimination between the two modes is essential to understanding macroscopic fluid transport and ultimately in determining strategies to improve drug delivery to solid tumors.

The time constants for these two processes arise naturally when tissue deformation is considered to be analogous to solute diffusion with chemical reaction. From a scaling analysis of Eq. 15 it follows that the characteristic time for fluid percolation through the interstitium is

$$\tau_i \propto R^2/\tilde{K}(2\tilde{\mu} + \tilde{\lambda})$$

and that for fluid filtration across the vessel wall is

$$\tau_v \propto \frac{1}{(2\tilde{\mu}+\tilde{\lambda})\dfrac{\tilde{L}_p S}{V}};$$

thus, the parameter $\tilde{\alpha}$ also represents the ratio of the two: $\tilde{\alpha} \propto \tau_i/\tau_v$. The exact value of this time constant can be evaluated analytically for the case of a step change of microvascular pressure, where the relaxation time for fluid pressure and velocity (as well as solid dilatation and displacement) is

$$\tau = \frac{R^2/\tilde{K}(2\tilde{\mu}+\tilde{\lambda})}{\tilde{\alpha}^2+\pi^2} \quad \text{(see Eq. A10)}$$

Therefore, τ reduces to τ_v in the limit $\tilde{\alpha}^2/\pi^2 \gg 1$ (fluid redistribution is dominated by the transvascular mode) and to τ_i when $\tilde{\alpha}^2/\pi^2 \ll 1$ (percolation dominates) as shown in Figure 2. It is worth noting that, unlike the percolation time constant, the time constant for transcapillary fluid exchange does not depend on the radius of the tumor, indicating that, on the macroscopic scale, transcapillary fluid exchange becomes more dominant in large tumors (i.e., the ratio α increases with R).

From the physiological data listed in Table 1, it is possible to estimate the parameter $\tilde{\alpha}$ and corresponding characteristic times for a solid tumor: $\tilde{\alpha}^2/\pi^2 \approx 160$,

$$\tau_i = \frac{R^2}{\pi^2\tilde{K}(2\tilde{\mu}+\tilde{\lambda})} \approx 1{,}000 \text{ s}$$

and

$$\tau_v = \frac{1}{(2\tilde{\mu}+\tilde{\lambda})\dfrac{\tilde{L}_p S}{V}} \approx 10 \text{ s}.$$

These values indicate that transvascular exchange has the smaller resistance to fluid transport in a solid tumor so that the fluid redistribution will be determined by a transvascular regime and thus the time constant will be on the order of 10 s (Figures 3 and 4). However, if the transcapillary exchange pathway is somehow shut off percolation would represent the only possible mechanism for fluid to leave the tumor. In this case the evolution of IFP and fluid velocity, described by Eqs. A10 and A12 reported in the Appendix, will occur over a time scale of thousands of seconds (Figure 5). These model predictions have been corroborated experimentally (Netti et al., 1995).

The notion of considering the vascular system as a distribution system of source and sink points is similar to some previous analyses in which the vascular network itself is regarded as another porous medium embedded in the tissue. Theoretical solutions and simulations along these lines have been presented by Huyghe et al. (1992, 1989a,b).

Microscopic analysis

Steady State. As the parameter $\tilde{\alpha}$ controls the average IFP and fluid-velocity profiles on a macroscopic scale, the local parameter α_L determines the local distributions of interstitial fluid pressure and velocity (Figure 7). The value of α_L estimated using the parameters of Table 1 ranges between 0.01 and 0.1, which indicates that in contrast to the macroscopic level, transcapillary resistance controls the perivascular fluid flow. Therefore, the understanding of the relevant fluid-transport parameters for the system as a whole requires an integrated macro- and microscopic analysis.

Transient Process. When the vascular pressure is changed rapidly, a redistribution of fluid flow in the interstitium follows. At the macroscopic level this process evolves over a time scale characteristic of transvascular fluid exchange:

$$\tau_v = \frac{1}{(2\tilde{\mu}+\tilde{\lambda})\dfrac{\tilde{L}_p S}{V}}.$$

The characteristic time scale for the local evolution of the fluid pressure is

$$\tau_l = \frac{(\Delta/2)^2}{(2\tilde{\mu}+\tilde{\lambda})\tilde{K}}.$$

These two time scales are not necessarily the same and should coincide only in the ideal case of no heterogeneity in local transport parameters (L_p, K) and homogeneous distribution of vessels. By comparing the macroscopic and microscopic time scales, we can estimate an average distance between blood vessels, $\Delta = 2(R/\tilde{\alpha}) \approx 500$ μm, which is consistent with the postulated hypothesis of noninteractive vessels. In reality, tumor vascular density is extremely heterogeneous (Jain, 1994). Hypoxic or necrotic areas, for example, present a much larger intercapillary distance compared to the more dense vascular areas. As a result, the local pressure evolution may occur on a different time scale than that of the macroscopic distribution. In the case of $\tau_l < \tau_v$ (dense vascular area), the perivascular flow is unidirectional (Figure 8A), whereas in the case of $\tau_l > \tau_v$, the IFP may be transiently higher than the vascular pressure, and the perivascular flow may change direction (Figure 8B).

In the microscopic model presented here only radial pressure gradients have been considered. A detailed analysis of perivascular fluid flow would require rigorously coupling Darcy's law for interstitial flow with Navier–Stokes equation for vascular flow. However, the main focus of our study was to analyze the effect of a heterogeneous distribution of vascular pressure on perivascular fluid flow and, in particular, the interaction between the microscopic and macroscopic fields. For this purpose, the axial pressure can be averaged out along the blood vessel since, due to low values of L_p and K, its gradient is negligible compared to the radial pressure gradient (Apelblat et al., 1974). This approximation is even more legitimate in tumors since the axial pressure gradient is reduced compared to normal tissues (Netti et al., 1996; Baish et al., 1997).

Sensitivity analysis

Interstitial Hydraulic Conductivity. Hydraulic conductivity of tumor tissue was estimated from *in vitro* permeability experiments and *in vivo* studies. Measurements span a range of

three orders of magnitude (0.7 to 590×10^{-8} cm^2/mmHg·s) (Boucher et al., 1996; DiResta et al., 1993; Swabb et al., 1974). At the macroscopic level, the value of $\tilde{K}$ affects the parameter $\tilde{\alpha}$ and the interstitial percolation time constant τ_i. However, if $\tilde{\alpha} \gg 1$, $\tilde{K}$ does not play a determining role in the process of transient fluid redistribution following vascular pressure modulation. Also at the microscopic level K does not play a primary role in controlling the perivascular fluid velocity distribution (see Eq. 38).

It has been reported that tissue hydration has a strong influence on the value of $\tilde{K}$ in normal tissue (Levick, 1987; Mow et al., 1986), and this may also be true in tumor tissue (Jain, 1987b; Levick, 1987; Swabb et al., 1974). Although the range of IFP considered here does not lead to high dilatation of the tissue, and therefore the variation of hydration is fairly small (Eq. 17 predicts that an increase in hydrostatic pressure of 10 mmHg leads to only a 1% increase in tissue hydration), the functional relationships that have been suggested between $\tilde{K}$ and hydration (Jackson and James, 1982; Lai and Mow, 1980) could be introduced in this model in cases where this effect is important.

Vascular Hydraulic Conductivity. The hydraulic permeability of the vascular wall ($\tilde{L}_p$) plays a primary role in controlling the transient fluid redistribution in tumors. Measurements of $\tilde{L}_p$ in normal tissue, obtained by a single capillary perfusion technique (Michel et al., 1974), are quite scattered and span a range of 1 to 30×10^{-7} cm/mmHg·s (Levick and Michel, 1977), depending on the location and age of the vessel. Within the same vessel $\tilde{L}_p$ does not vary with vascular pressure (Levick and Michel, 1977). Direct measurements of $\tilde{L}_p$ in tumor vessels are not available to date, although there is experimental evidence that suggests that $\tilde{L}_p$ is higher and more heterogeneous in tumors compared to normal tissues (Jain and Baxter, 1993; Sevick and Jain, 1991; Yuan et al., 1993). The variability of $\tilde{L}_p$ may cause differences in the time constant for redistribution of macroscopic IFP among different tumors and, within a tumor, regional variations may also occur. Therefore the value of $\tilde{L}_p$ used in the simulation should be regarded as an average over all vessels within the tumor mass.

On the microscopic level, Eq. 38 indicates that L_p is the most important parameter controlling the perivascular velocity distribution.

Tissue Compliance. The tissue compliance does not affect the IFP profile in the steady state, but plays an important role in determining the characteristic transient time.

Vascular Density. The vascular density (S/V) controls the gross macroscopic vascular permeability. The value of this parameter ranges from 50 to 570 cm^{-1}, depending on the tumor type (Jain, 1987a). Moreover, in contrast to normal tissue, it has been shown that the vascular density in tumor tissue increases with transmural pressure (Hori et al., 1985), presumably due to the recruitment of redundant vessels in tumor tissues. Hori et al. (1985) reported a twofold increase in the vascular density with a 45% elevation of systemic pressure. In the physiological range of possible vascular pressure variations, it is reasonable to assume a linear dependence of the vascular density on the transmural pressure:

$$\frac{S}{V} = H(\tilde{p}_v - \tilde{p}) + H_o, \tag{45}$$

where H represents the rate of variation of vascular density and H_o is the vascular density at zero transmural pressure. Substituting Eq. 45 in Eq. 14, the resulting nonlinear PDE is no longer solvable analytically, although a numerical integration would be straightforward. A scaling analysis of the model equation leads to the following expression for the characteristic time constant incorporating Eq. 45:

$$\frac{1}{\tau} \propto (2\tilde{\mu} + \tilde{\lambda})\left[\tilde{L}_p(H\tilde{p}_v^o + H_o) + \frac{\tilde{K}}{R^2}\right] = \frac{1}{\tau_v} + \frac{1}{\tau_i}, \tag{46}$$

where $\tilde{p}_v^o$ is a reference transmural pressure (i.e., $\tilde{p}_v^o = \tilde{p}_v - \tilde{p}$). Since,

$$\tilde{\alpha} = R\sqrt{\frac{\tilde{L}_p(H\tilde{p}_v^o + H_o)}{\tilde{K}}} > 1,$$

the interstitial fluid redistribution following a step change of vascular pressure occurs on a time scale

$$\tau_v = \frac{1}{(2\tilde{\mu} + \tilde{\lambda})\tilde{L}_p(H\tilde{p}_v^o + H_o)}.$$

This result indicates that the characteristic time depends on the vascular pressure, that is, the transient time for an increase of vascular pressure is smaller than that relative to a corresponding decrease of the vascular pressure. It is worth noting that this conclusion has a general validity and does not depend on the particular functionality chosen for the vascular density (Eq. 46). The response of the system to a rapid change of vascular pressure is symmetric only if the vascular density is constant with the transmural pressure.

Implications for drug delivery

For any systemic therapy to be effective, a drug has to cross the vascular wall and penetrate at least half the intercapillary distance. Some useful characteristic times and dimensionless groups for perivascular transport processes are reported in Table 2. The consolidation time is the characteristic time for perivascular fluid redistribution. The characteristic time for advection depends on the parameters L_p, K, and the pressure difference ($p_v - \tilde{p}$). The relative importance of convection in macromolecular transport increases with the pressure difference ($p_v - \tilde{p}$). Assuming $p_v - \tilde{p} = 10$ mmHg, which is the maximum expected according to the data of Boucher and Jain (1992), the resulting Peclet number is approximately $P_e \cong (\tau_d/\tau_c) \cong 0.4$. This indicates that both convection and diffusion are important for interstitial transport, although the diffusion component becomes the predominant mechanism for small transmural pressure gradients ($p_v - \tilde{p}$).

Figure 9 shows the time period required for a particle of fluid to travel 100 μm from the blood vessel as a function of L_p and K. For low values of L_p, the penetration time is independent of K (Figure 9A); rather it depends strongly on L_p (Figure 9B). This indicates that transvascular transport is the main resistance that a macromolecule has to overcome to penetrate into a tumor and, as such, macromolecular uptake could be improved either by increasing L_p or the transmural pressure gradient.

Table 2. Relevant Time Constants for Perivascular Transport Processes

Process	Time Constant	Value (s)
Consolidation	$\tau_c = \dfrac{(\Delta/2)^2}{(2\mu+\lambda)K}$	~ 3.5
Diffusion	$\tau_d = \dfrac{(\Delta/2)^2}{D}$	~ 1,000
Advection	$\tau_a = \dfrac{(\Delta/2)^2}{\beta}$	$\sim \dfrac{270{,}000}{(p_v - \bar{p})}$

Note: $\beta = [L_p/1 + \alpha_L \ln(R/\rho)](p_v - p)\rho$.
All characteristic times are evaluated assuming a distance Δ of 200 μm. The diffusion time has been evaluated assuming $D = 10^{-7}$ cm^2/s, which is characteristic for monoclonal antibody (IgG) of 150,000 Dalton (Berk et al., 1996).

Since the average IFP in the center of the tumor is close to the average vascular pressure in the steady state (see Eq. 31), there is little driving force for fluid and macromolecular extravasation (Eq. 39). An increase of fluid extravasation occurs when the vascular pressure is increased (Figure 8), but this enhanced extravasation is only temporary, since a parallel increase of the average IFP follows within approximately 10 s (Figure 4). This short time is insufficient in producing any net appreciable increase of uptake or drug concentration in the interstitium. Specifically, the quantity of drug per unit volume of tissue ($\Delta\tilde{C}$) that extravasates by convection following a rapid increase of vascular pressure can be calculated as

$$\Delta\tilde{C} = (1 - \tilde{\sigma}_F)\frac{\tilde{L}_p S}{V}\tilde{C}_p \pi \int_0^{\infty}\int_0^{R}(\tilde{p}_v - \tilde{p})r^2\,dr\,dt, \quad (47)$$

where $\tilde{C}_p$ is the average plasma concentration, $\tilde{\sigma}_F$ is the solvent-drag reflection coefficient, and $(1 - \tilde{\sigma}_F)$ is a measure of the coupling between fluid and solute transport (Kedem and Katchalsky, 1961). Since tumor blood vessels are characterized by large pore size ($O(1\ \mu m)$) (Hobbs et al., 1996) and the Stokes–Einstein radius of typical macromolecular agents (e.g., monoclonal antibodies) is $O(10$ nm) (Yuan et al., 1995), the coefficient $\tilde{\sigma}_F$ can be assumed to be zero as a first approximation. The relative increase of average interstitial concentration is

$$\frac{\tilde{C}_i^f}{\tilde{C}_i^o} = \frac{\tilde{C}_i^o + \Delta\tilde{C}}{\tilde{C}_i^o}, \quad (48)$$

where $\tilde{C}_i^o$ and $\tilde{C}_i^f$ are the initial and final average interstitial drug concentrations. For a value of $\tilde{C}_p/\tilde{C}_i^o = 3$ (Baxter and Jain, 1991) and a doubling of the transvascular pressure, this increase is only 2%.

A more beneficial effect may be achieved by cycling the systemic blood pressure (Netti et al., 1995). In this case, each increase of vascular pressure there will result in an additional accumulation of drug in the interstitium. A rapid increase of vascular pressure leads to a transient increase of perivascular convection. Figure 10 shows the perivascular penetration of a fluid particle as a function of time. Following a rapid doubling of vascular pressure, the fluid particle would cover a distance of 20 μm from the blood vessel in 100 s, rather than the 10 μm it would cover in the same time period at steady state.

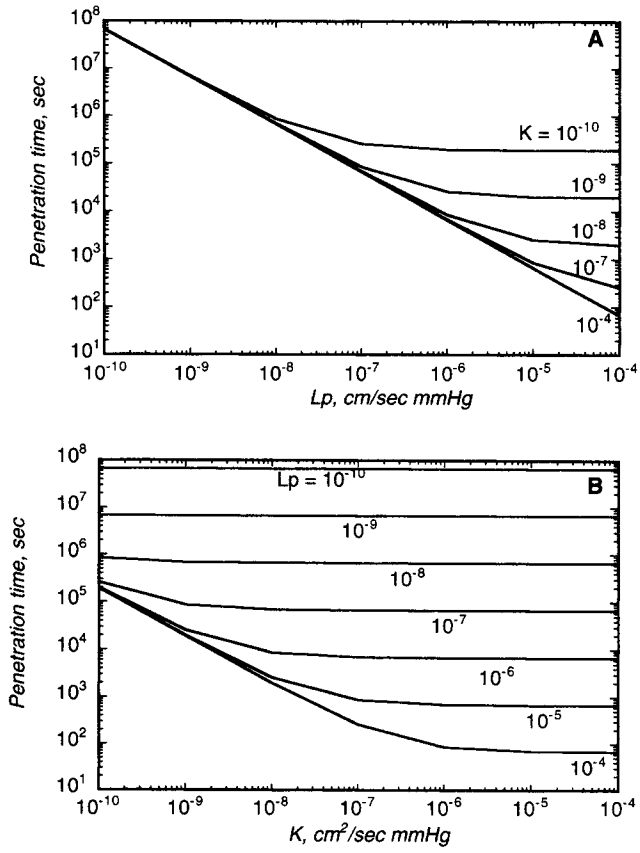

Figure 9. Sensitivity of the penetration time to K (A) and L_p (B).

The penetration time (time required to penetrate 100 μm in the tissue) is a weak function of the parameter K, especially for low value of L_p (A), whereas it is very sensitive to the value of L_p (B), indicating that the parameter L_p is crucial in controlling the convective component for drug delivery. Note that the physiological parameters reported in Table 1 ($L_p = 3.7\times10^{-10}$ cm/mm Hg·s and $K = 4.13\times10^{-8}$ cm^2/mm Hg·s), an increase of tissue hydraulic conductivity will not induce any appreciable increase of convective component, whereas an increase of L_p will be more effective.

A potential problem with this strategy is possible reabsorption of extravasated drug during the vascular pressure reduction phase. However, since the perivascular Peclet number is less than unity, diffusion will induce a spreading of extravasated drug in the interstitium. Moreover, under conditions of high binding affinity of the drug to cancer cells, the drug that extravasates in each hypertensive phase may not be reabsorbed in the successive normotensive phase. For example, monoclonal antibodies are specifically designed to avidly bind to tumor cells; their accumulation may be greatly enhanced by a periodic modulation of the systemic blood pressure. Cycling of blood pressure would be even more beneficial for improving the penetration of all the macromolecular drugs in those tumors with redundant blood vessels. In this case, the reduction of the draining capacity of the blood vessels due to a reduction in vascular density (S/V) during a decrease of vascular pressure may force an interstitial circulation of fluid.

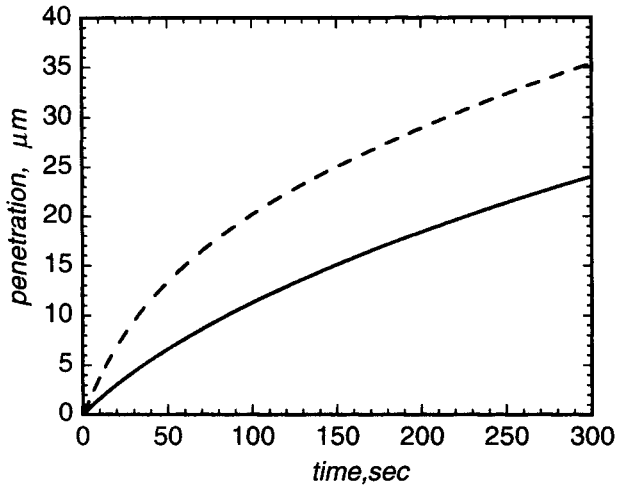

Figure 10. Perivascular penetration of a fluid particle as a function of time in steady state (——) and following a rapid change of vascular pressure (---).

As a consequence of a rapid increase of the vascular pressure, there is an acceleration of the perivascular fluid particles; the perivascular penetration after 100 s is 10 μm in the steady state and 20 μm following a rapid increase (doubling) of the vascular pressure.

The preceding analysis regards only the convective component of transvascular transport. The diffusive component is not taken into account because, due to the low diffusion coefficient of macromolecular drugs considered here, the extravasation is thought to occur mainly by convection (Flessner and Dedrick, 1994; Rippe et al., 1978).

Conclusion

We have applied poroelastic theory to describe the fluid-transport process in living tissue, at both macroscopic and microscopic scales. The coupling between transvascular and interstitial fluid flow has been described by incorporating a fluid source term in the macroscopic mass balance. This type of analysis has been useful in identifying physiological parameters that control the steady state as well as the transient distribution of interstitial fluid, and represents a valuable tool for the estimation of these parameters *in vivo*.

By applying this analysis to solid tumors, we have described the macroscopic and microscopic IFP and fluid-velocity profiles. At the macroscopic level, the major barrier to fluid transport was found to be the interstitial resistance, whereas the transvascular resistance turned out to be the major transport barrier at the microscopic level. The model successfully predicted the steady-state and transient IFP profiles and fluid velocity in solid tumors using physiological parameters reported in the literature. The implications of the model have suggested possible strategies to improve macromolecular uptake (i.e., cycling arterial blood pressure), and we hope that other therapeutic strategies can benefit from this study.

Acknowledgment

This work was supported by an Outstanding Investigator Grant from the National Cancer Institute (R35-CA-56591) (R. K. J.). Another author (P. A .N.) was supported in part by the Italian National Research Council (CNR).

Notation

Macroscopic (average) variables and parameters

$\tilde{C}_p$ = macromolecular concentration in plasma, g/mL
$\tilde{C}_i^0, \tilde{C}_i^f$ = macromolecular concentration in interstitial fluid, g/mL
D = interstitial diffusion coefficient, cm^2/s
$\tilde{\Omega}$ = fluid source term per volume of tissue, s^{-1}
e = solid matrix dilatation
$\tilde{e}$ = solid matrix dilatation
K = interstitial hydraulic permeability, cm^2/mm Hg·s
$\tilde{K}$ = interstitial hydraulic permeability, cm^2/mm Hg·s
L_p, L_{pL} = hydraulic permeability of the vascular and lymphatic wall cm^2/mm Hg·s
$\tilde{L}_p$, $\tilde{L}_{pL}$ = hydraulic permeability of the vascular and lymphatic wall cm^2/mm Hg·s
p = interstitial fluid pressure (IFP)
$\tilde{p}$ = interstitial fluid pressure (IFP)
$\tilde{p}_c$ = interstitial fluid pressure (IFP)
$\tilde{p}_L$ = lymphatic pressure, mm Hg
$\tilde{p}_o$, $\tilde{p}_v$ = actual and reference effective vascular pressure, mm Hg
$\tilde{\rho}_s$, $\tilde{\rho}_f$ = solid and fluid mass density, g/cm^3
Pe = interstitial Peclet number
R = tumor radius, cm
r = macroscopic spatial coordinate, cm
r_0 = perivascular penetration depth (distance from blood vessel at which local variables approach mean field value)
S/V, S_L/V = capillary and lymphatic surface density, cm^{-1}
u = solid matrix displacement μm
$\tilde{u}$ = solid matrix displacement μm
v = interstitial fluid velocity, μm/s
$\tilde{v}$ = interstitial fluid velocity, μm/s
V_t, V_t^o = deformed and undeformed tissue volume, cm^3
$x = (\frac{\tilde{p}_v^{\text{fin}}}{\tilde{p}_o})$ = ratio of final to initial effective vascular pressure
$\alpha_L = L_p \rho$ = ratio of K transvascular to interstitial fluid transport resistance
Δ = intercapillary distance, μm
ϕ, ϕ^o = transient, actual and reference tissue hydration
ϕ, ϕ^o = transient, actual and reference tissue hydration
$\delta\Gamma$ = volume of an elementary piece of tissue, cm^3
ϵ = matrix deformation tensor
$\underline{\tilde{\epsilon}}$ = matrix deformation tensor
ρ = capillary radius, μm
$\tilde{\varphi}_v$, $\tilde{\varphi}_L$ = vascular and lymphatic fluid flow per volume of tissue (s^{-1})
μ, λ = Lame' constants for solid matrix, mm Hg
$\tilde{\mu}$, $\tilde{\lambda}$ = Lame' constants for solid matrix, mm Hg
ξ = perivascular spatial coordinate, μm
$\tilde{\pi}_c$, $\tilde{\pi}_i$ = interstitial and vascular osmotic pressure, mm Hg
$\tilde{\sigma}$ = vascular reflection coefficient
τ = solid stress tensor, mm Hg
$\tilde{\tau}$ = solid stress tensor, mm Hg

Literature Cited

An, K. N., and E. P. Salathe, "A Theory of Interstitial Fluid Motion and Its Implication for Capillary Exchange," *Microvasc. Res.*, **12**, 103 (1976).

Apelblat, A., A. K. Katchalsky, and A. Silberberg, "A Mathematical Analysis of Capillary-Tissue Fluid Exchange," *Biorheology*, **11**, 1 (1974).

Baish, J., P. A. Netti, and R. K. Jain, "Transmural Coupling of Fluid Flow in Microcirulatory Network and Interstitium in Tumors," *Microvascular Res.* (in press, 1997).

Barocas, V. H., D. M. Knapp, and R. T. Tranquillo, "Biphasic Mechanical Theory for Fibrillar Gels," *Proc. ASME Bioengineering Meeting*, **BED-29**, ASME, Beaver Creek, CO, p. 309 (1995).

Basser, P. J., "Interstitial Pressure, Volume and Flow During Infusion into Brain Tissue," *Microvasc. Res.*, **44**, 143 (1992).

Baxter, L. T., and R. K. Jain, "Transport of Fluid and Macromolecules in Tumors. I. Role of Interstitial Pressure and Convection," *Microvasc. Res.*, **37**, 77 (1989).

Baxter, L. T., and R. K. Jain, "Transport of Fluid and Macro-

molecules in Tumors III. Role of Binding and Metabolism," *Microvasc. Res.*, **41**, 5 (1991).
Berk, D. A., F. Yuan, M. Leunig, and R. K. Jain, "Direct in vivo Measurement of Targeted Binding in Human Tumor Xenograft," *Proc. Natl. Acc. Sci.* (in press, 1997).
Biot, M. A., "General Theory of Three-Dimensional Consolidation," *J. Appl. Phys.*, **12**, 155 (1941).
Biot, M. A., "Theory of Elasticity and Consolidation for a Porous Anisotropic Solid," *J. Appl. Phys.*, **26**, 182 (1955).
Boucher, Y., L. T. Baxter, and R. K. Jain, "Interstitial Pressure Gradients in Tissue-Isolated and Subcutaneous Tumors: Implications for Therapy," *Cancer Res.*, **50**, 4478 (1990).
Boucher, Y., C. Brekken, P. A. Netti, L. T. Baxter, and R. K. Jain, "Hydraulic Conductivity and Compliance of Solid Tumors: A Novel Measurement Technique and Implication for Drug Delivery," (1996).
Boucher, Y., and R. K. Jain, "Microvascular Pressure is the Principal Driving Force for Interstitial Hypertension in Solid Tumors: Implication for Vascular Collapse," *Cancer Res.*, **52**, 5110 (1992).
Bowen, R. M., "Theory of Mixtures," *Continuum Physics*, Vol. III, A. C. Eringen, ed., Academic Press, New York, p. 1 (1976).
Bowen, R. M., "Incompressible Porous Media Models by Use of the Theory of Mixtures," *Int. J. Eng. Sci.*, **18**, 1129 (1980).
DiResta, G. R., J. Lee, S. M. Larson, and E. Arbit, "Characterization of Neuroblastoma Xenograft in Rat Flank. I. Growth, Interstitial Fluid Pressure, and Interstitial Fluid Velocity Distribution Profile," *Microvasc. Res.*, **46**, 158 (1993).
Flessner, M. F., and R. L. Dedrick, "Monoclonal Antibody Delivery to Intraperitoneal Tumors in Rats: Effect of Route of Administration and Intraperitoneal Osmolarity," *Cancer Res.*, **54**, 4376 (1994).
Fung, Y. C., *Biomechanics: Motion, Flow, Stress, and Growth*, Springer-Verlag, New York (1990).
Grimshaw, P. E., A. J. Grodzinksy, M. L. Yarmush, and D. M. Yarmush, "Dynamic Membranes for Protein Transport: Chemical and Electrical Control," *Chem. Eng. Sci.*, **44**, 827 (1989).
Gullino, P. M., "Extracellular Compartment of Solid Tumors," *Cancer*, F. F. Becker, ed., Plenum Press, New York (1975).
Hilmas, D., and E. L. Gilette, "Morphometric Analyses of the Microvasculature of Tumors During Growth and After X-Irradiation," *Cancer*, **33**, 103 (1974).
Hobbs, S. K., F. Yuan, L. G. Cima, and R. K. Jain, "Tumor Vasculature Pore Cutoff Size: Implications for Macromolecular and Particle Drug Delivery," *Int. J. Microcirc. Clin. Exp. (Suppl. 1)*, p. 396 (1996).
Holmes, M. H., "Finite Deformation of Soft Tissue: Analysis of a Mixture Model in Uniaxial Compression," *J. Biomech. Eng.*, **108**, 372 (1986).
Holmes, M. H., W. M. Lai, and V. C. Mow, "Singular Perturbation Analysis of the Nonlinear, Flow-Dependent, Compressive Stress-Relaxation Behavior of Articular Cartilage," *J. Biomech. Eng.*, **107**, 206 (1985).
Hori, K., M. Suzuki, I. Abe, S. Saito, and H. Sato, "Increase in Tumor Vascular Area Due to Increased Blood Flow by Angiotensin II in Rats," *J. Nat. Cancer Inst.*, **74**, 453 (1985).
Huyghe, J. M., T. Arts, and D. H. van Campen, "Porous Medium Finite Element Model of the Beating Left Ventricle," *Amer. J. Physiol.*, **262**, H1256 (1992).
Huyghe, J. M., C. W. Oomens, and D. H. van Campen, "Low Reynolds Number Steady State Flow Through a Branching Network of Rigid Vessel: II. A Finite Element Mixture Theory," *Biorheology*, **26**, 73 (1989a).
Huyghe, J. M., C. W. Oomens, D. H. van Campen, and R. M. Heethaar, "Low Reynolds Number Steady State Flow Through a Branching Network of Rigid Vessel: I. A Mixture Theory," *Biorheology*, **26**, 55 (1989b).
Jackson, G. W., and D. F. James, "The Hydrodynamic Resistance of Hyaluronic Acid and Its Contribution to Tissue Permeability," *Biorheology*, **19**, 317 (1982).
Jain, R. K., "Transport of Molecules Across Tumor Vasculature," *Cancer Metastasis Rev.*, **6**, 559 (1987a).
Jain, R. K., "Transport of Molecules in the Tumor Interstitium: A Review," *Cancer Res.*, **47**, 3039 (1987b).
Jain, R. K., "Determinants of Tumor Blood Flow: A Review," *Cancer Res.*, **48**, 2641 (1988).
Jain, R. K., "Transport Phenomena in Tumors," *Adv. Chem. Eng.*, **19**, 129 (1994).
Jain, R. K., "Delivery of Molecular Medicine to Solid Tumors," *Science*, **271**, 1079 (1996a).
Jain, R. K., "Delivery of Molecules, Particles, and Cells to Solid Tumors," *Ann. Biomed. Eng.*, **24**, 457 (1996b).
Jain, R. K., and L. T. Baxter, "Mechanism of Heterogeneous Distribution of Monoclonal Antibodies and Other Macromolecules in Tumors: Significance of Elevated Interstitial Pressure," *Cancer Res.*, **48**, 7022 (1988).
Jain, R. K., and L. T. Baxter, "Extravasation and Interstitial Transport in Tumors," *Biological Barriers to Protein Delivery*, L. A. Kenneth and J. R. Thomas, eds., Plenum Press, New York, p. 441 (1993).
Jain, R., and G. Jayaraman, "A Theoretical Model for Water Flux through the Arterial Wall," *J. Biomech. Eng.*, **109**, 311 (1987).
Jain, R. K., J. M. Weissbrod, and J. Wei, "Mass Transport in Tumor: Characterization and Application to Chemotherapy," *Advances in Cancer Research*, G. Klein and S. Weinhouse, eds., Academic Press, New York, p. 251 (1980).
Kedem, O., and A. Katchalsky, "A Physical Interpretation of the Phenomenological Coefficients of Membrane Permeability," *J. Gen. Physiol.*, **45**, 143 (1961).
Keynton, D. E., "Transient Filtration in a Porous Elastic Cylinder," *Trans. ASME J. Appl. Mech.*, **98**, 594 (1976).
Krogh, A., *The Anatomy and Physiology of Capillaries*, 2nd ed., Yale Univ. Press, New Haven, CT (1922).
Lai, M. W., and V. C. Mow, "Drag-Induced Compression of Articular Cartilage During a Permeation Experiment," *Biorheology*, **17**, 111 (1980).
Levick, J. R., "Flow Through Interstitium and Other Fibrous Matrices," *Q. J. Exp. Physiol.*, **72**, 409 (1987).
Levick, J. R., and C. C. Michel, "A Densitometric Method for Determining the Filtration Coefficients of Single Capillaries in the Frog Mesentery," *Microvasc. Res.*, **13**, 141 (1977).
Mak, A. F., "The Apparent Viscoelastic Behavior of Articular Cartilage—The Contributions from the Intrinsic Matrix Viscoelasticity and Interstitial Flows," *J. Biomech. Eng.*, **108**, 123 (1986).
Michel, C. C., J. C. Mason, F. E. Curry, and J. E. Tooke, "A Development of the Landis Technique for Measuring the Filtration Coefficient of Individual Capillaries in the Frog Mesentery," *Q. J. Exp. Physiol.*, **59**, 283 (1974).
Mow, V. C., S. C. Kuei, W. M. Lai, and C. G. Armstrong, "Biphasic Creep and Stress Relaxation of Articular Cartilage in Compression: Theory and Experiments," *J. Biomech. Eng.*, **102**, 73 (1980).
Mow, V. C., M. K. Kwan, W. M. Lai, and M. H. Holmes, "A Finite Deformation Theory for Nonlinearly Permeable Soft Hydrated Biological Tissues," *Frontiers in Biomechanics*, S. Schmid-Schonbein, L.-Y. Woo, and B. W. Zweifach, eds., Springer-Verlag, New York (1986).
Mow, V. C., and W. M. Lai, "Mechanics of Animal Joints," *Annu. Rev. Fluid Mech.*, M. Van Dyke, ed., **11**, 247 (1979).
Nagashima, T., T. Shirakuni, and S. I. Rapoport, "A Two Dimensional Finite Element Analysis of Vasogenic Brain Edema," *Neurol. Med.-Chir. (Tokyo)*, **30**, 1 (1990).
Nagashima, T., N. Tamaki, S. Matsumoto, B. Horwitz, and Y. Seguchi, "Biomechanics of Hydrocephalus: A New Mathematical Model," *Neurosurgery*, **21**, 898 (1987).
Netti, P. A., L. T. Baxter, Y. Boucher, R. Skalak, and R. K. Jain, "Time-Dependent Behavior of Interstitial Fluid Pressure in Solid Tumors: Implication for Drug Delivery," *Cancer Res.*, **55**, 5451 (1995).
Netti, P. A., S. Roberge, Y. Boucher, L. T. Baxter, and R. K. Jain, "Effect of Transvascular Fluid Exchange on Pressure-Flow Relationship in Tumors: A Proposed Mechanism for Tumor Blood Flow Heterogeneity," *Microvasc. Res.*, **52**, 27 (1996).
Nicholson, C., and J. M. Phillips, "Ion Diffusion Modified by Tortuosity and Volume Fraction in the Extracellular Environment of Rat Cerebellum," *J. Physiol.*, **321**, 225 (1981).
Rippe, B., A. Kamiya, and B. Folkow, "Simultaneous Measurements of Capillary Diffusion and Filtration Exchange During Shifts in Filtration-Absorption and at Graded Alterations in the Capillary Permeability Surface Area Product (PS)," *Acta Physiol. Scand.*, **104**, 318 (1978).

Salathe, E. P., and K. N. An, "A Mathematical Analysis of Fluid Movement Across Capillary Walls," *Microvasc. Res.*, **11**, 1 (1976).
Sevick, E. M., and R. K. Jain, "Measurement of Capillary Filtration Coefficient in a Solid Tumor," *Cancer Res.*, **51**, 1352 (1991).
Simon, B. R., "Multiphase Poroelastic Finite Element Models for Soft Tissue Structure," *Appl. Mech. Rev.*, **45**, 191 (1992).
Simon, B. R., and M. Gaballa, "Finite Strain Poroelastic Finite Element Models for Large Arterial Cross Sections," *Computational Methods in Bioengineering*, R. L. Spilker and B. R. Simon, eds., ASME, New York, p. 325 (1988a).
Simon, B. R., and M. Gaballa, "Poroelastic Finite Element Models for the Spinal Motion Segment Including Ionic Swelling," *Computational Methods in Bioengineering*, R. L. Spilker and B. R. Simon, eds., ASME, New York, p. 93 (1988b).
Simon, B. R., J. S. S. Wu, and J. H. Evans, "Poroelastic Mechanical Models for the Intervertebral Disc," *Proc. ASME Winter Annual Meeting*, D. Bartel, ed., Boston, p. 106 (1983).
Spilker, R. L., and J. K. Suh, "Formulation and Evaluation of a Finite Element Model for the Biphasic Model of Hydrated Soft Tissue," *Comput. Struct.*, **35**, 425 (1990).
Spilker, R. L., J. K. Suh, and V. C. Mow, "A Finite Element Analysis of Indentation Stress-Relaxation Response of Linear Biphasic Articular Cartilage," *J. Biomech. Eng.*, **114**, 192 (1992).
Swabb, E. A., J. Wei, and P. M. Gullino, "Diffusion and Convection in Normal and Neoplastic Tissues," *Cancer Res.*, **34**, 2814 (1974).
Tanaka, T., and D. J. Fillmore, "Kinetics of Swelling of Gels," *J. Chem. Phys.*, **70**, 1214 (1978).
Truesdell, C., and R. A. Toupin, "The Classical Field Theories," *Handbuck der Physik*, Vol. III/I, Springer, Berlin (1960).
Yuan, F., M. Dellian, D. Fukumura, M. Leunig, D. A. Berk, V. P. Torchilin, and R. K. Jain, "Vascular Permeability in a Human Tumor Xenograft: Molecular Size Dependence and Cutoff Size," *Cancer Res.*, **55**, 3752 (1995).
Yuan, F., M. Leunig, D. A. Berk, and R. K. Jain, "Microvascular Permeability of Albumin, Vascular Surface Area and Vascular Volume Measured in Human Adenocarcinoma LS174T Using Dorsal Chamber in SCID Mice," *Microvasc. Res.*, **45**, 269 (1993).
Zlotecki, R. A., L. T. Baxter, Y. Boucher, and R. K. Jain, "Pharmacological Modification of Tumor Blood Flow and Interstitial Fluid Pressure in a Human Tumor Xenograft: Network Analysis and Mechanistic Interpretation," *Microvasc. Res.*, **50**, 429 (1995).
Zlotecki, R. A., Y. Boucher, I. Lee, L. T. Baxter, and R. K. Jain, "Effect of Angiotensin II Induced Hypertension on Tumor Blood Flow and Interstitial Fluid Pressure," *Cancer Res.*, **53**, 2466 (1993).

Appendix

Change in microvascular pressure

To solve the transient fluid-transport problems it is convenient to rewrite Eq. 25 in terms of variations with respect to the initial steady state. [Note: hereafter deviations from the steady state are marked with an asterisk (*), that is, $\tilde{e}^* = \tilde{e}(r,t) - \tilde{e}(r,0)$]:

$$\frac{\partial \tilde{e}^*}{\partial \hat{t}} - \frac{1}{\hat{r}^2}\frac{\partial}{\partial \hat{r}}\left(\hat{r}^2 \frac{\partial \tilde{e}^*}{\partial \hat{r}}\right) + \tilde{\alpha}^2 \tilde{e}^* = \tilde{\alpha}^2 \tilde{p}_f^*, \qquad \text{(A1)}$$

where

$$\tilde{p}_f^* = \frac{\tilde{p}_o - \tilde{p}_v}{2\tilde{\mu} + \tilde{\lambda}}.$$

The initial condition for tissue dilation starting from the initial steady state is $\tilde{e}^*(\hat{r},0) = 0$. Applying the Laplace transform to Eq. A1:

$$\frac{\partial^2 \bar{\tilde{e}}^*}{\partial \hat{r}^2} + \frac{2}{\hat{r}}\frac{\partial \bar{\tilde{e}}^*}{\partial \hat{r}} - (\tilde{\alpha}^2 + s)\bar{\tilde{e}}^* = \tilde{\alpha}^2 \bar{\tilde{p}}_f^*, \qquad \text{(A2)}$$

where s is the transform variable. Using modified spherical Bessel functions and integrating,

$$\bar{\tilde{e}}^* = \frac{\alpha^2 \bar{\tilde{p}}_f^*}{\tilde{\beta}^2}\left(\frac{\sinh(\tilde{\beta}\hat{r})}{\hat{r}\sinh(\tilde{\beta})} - 1\right), \qquad \text{(A3)}$$

where $\tilde{\beta} = \sqrt{\tilde{\alpha}^2 + s}$.

The transient pressure distribution can be derived using Eq. 24:

$$\bar{\tilde{p}}^* = (2\tilde{\mu} + \tilde{\lambda})\frac{\tilde{\alpha}^2 \bar{\tilde{p}}_f^*}{\tilde{\beta}^2}\left(\frac{\sinh(\tilde{\beta}\hat{r})}{\hat{r}\sinh(\tilde{\beta})} - 1\right), \qquad \text{(A4)}$$

and the interstitial displacement is derived using Eq. 8:

$$\bar{\tilde{u}}^* = \frac{\tilde{\alpha}^2 \bar{\tilde{p}}_f^*}{\tilde{\beta}^2}\left(\frac{\tilde{\beta}\hat{r}\cosh(\tilde{\beta}\hat{r}) - \sinh(\tilde{\beta}\hat{r})}{\tilde{\beta}^2\hat{r}^2\sinh(\tilde{\beta})} - \frac{\hat{r}}{3}\right). \qquad \text{(A5)}$$

Finally from Eq. 5 the transient fluid velocity can be expressed as

$$\bar{\tilde{v}}^* = (2\tilde{\mu} + \tilde{\lambda})\frac{\tilde{K}\tilde{\alpha}^2 \bar{\tilde{p}}_f^*}{\tilde{\phi}\tilde{\beta}^2}\left(\frac{\tilde{\beta}\hat{r}\cosh(\tilde{\beta}\hat{r}) - \sinh(\tilde{\beta}\hat{r})}{\hat{r}^2\sinh(\tilde{\beta})}\right) + s\frac{c\tilde{\alpha}^2 \bar{\tilde{p}}_f^*}{R^2\tilde{\beta}^2}\left(\frac{\tilde{\beta}\hat{r}\cosh(\tilde{\beta}\hat{r}) - \sinh(\tilde{\beta}\hat{r})}{\tilde{\beta}^2\hat{r}^2\sinh(\tilde{\beta})} - \frac{\hat{r}}{3}\right). \qquad \text{(A6)}$$

Equations A3–A6 constitute the general solution of the model in Laplace transform space. The transform must be inverted for each particular choice of the forcing function $\tilde{p}_f^*$, representing a given perturbation of vascular pressure. We will derive the solution for a step change in $\tilde{p}_f^*$; solutions for other forcing functions can be obtained by a convolution integral.

A step change in microvascular pressure can be formalized as

$$\tilde{p}_v = \tilde{p}_o[1 - (1-x)\cdot H(t)], \qquad \text{(A7)}$$

where $H(t)$ is the step function and $x = (\tilde{p}_v^{fin}/\tilde{p}_o)$ is the ratio of the final value of the vascular pressure to its initial value. The Laplace transform of Eq. A7 is

$$\bar{\tilde{p}}_v = \frac{x\tilde{p}_o}{s}$$

which leads to

$$\bar{\tilde{p}}_f^* = \frac{(1-x)}{(2\tilde{\mu} + \tilde{\lambda})}\frac{\tilde{p}_o}{s}. \qquad \text{(A8)}$$

The inverse transforms of Eqs. A3–A6, respectively, are

$$\tilde{e}^*(\hat{r},\hat{t}) = \frac{\tilde{\alpha}^2 \tilde{p}_o}{(2\tilde{\mu} + \tilde{\lambda})}\frac{(1-x)}{\hat{r}}\sum_{n=1}^{\infty}\frac{2}{n\pi}(-1)^n c_n(1 - e^{-f_n\hat{t}}) \qquad \text{(A9)}$$

$$\tilde{p}^*(\hat{r},\hat{t}) = \tilde{\alpha}^2\tilde{p}_o\frac{(1-x)}{\hat{r}}\sum_{n=1}^{\infty}\frac{2}{n\pi}(-1)^n c_n(1-e^{-f_n\hat{t}}) \quad \text{(A10)}$$

$$\tilde{u}^*(\hat{r},\hat{t}) = \frac{R\tilde{\alpha}^2\tilde{p}_o}{(2\tilde{\mu}+\tilde{\lambda})}\frac{(1-x)}{\hat{r}^2}\sum_{n=1}^{\infty}\frac{2}{n\pi}(-1)^n \times\frac{c_n - n\pi\hat{r}d_n}{n^2\pi^2}(1-e^{-f_n\hat{t}}) \quad \text{(A11)}$$

$$\tilde{v}^*(\hat{r},\hat{t}) = \frac{\tilde{K}\tilde{\alpha}^2\tilde{p}_o}{R\tilde{\phi}}\frac{(1-x)}{\hat{r}^2}\sum_{n=1}^{\infty}\frac{2}{n\pi}(-1)^n \times\frac{c_n - n\pi\hat{r}d_n}{n\pi}(1-e^{-f_n\hat{t}}) + \frac{\tilde{K}\tilde{\alpha}^2\tilde{p}_o}{R\tilde{\phi}}\frac{(1-x)}{\hat{r}^2}\sum_{n=1}^{\infty}\frac{2}{n\pi}(-1)^n \times\frac{c_n - n\pi\hat{r}d_n}{n^2\pi^2}f_n e^{-f_n\hat{t}}, \quad \text{(A12)}$$

where

$$c_n = \frac{\sin(n\pi\hat{r})}{n^2\pi^2+\tilde{\alpha}^2} \qquad d_n = \frac{\cos(n\pi\hat{r})}{n^2\pi^2+\tilde{\alpha}^2} \qquad f_n = (n^2\pi^2+\tilde{\alpha}^2).$$

Change in vascular flow

Here we will consider the case of an abrupt cessation of vascular flow as it occurs in response to circulatory arrest. This can be modeled as a step decrease of the generation term $\Omega(\hat{r},t)$ to zero:

$$\Omega(\hat{r},t) = \Omega_o[1-H(t)]. \quad \text{(A13)}$$

Using this as the forcing function in the transform of Eq. 19, we have

$$\frac{\partial^2\bar{\tilde{e}}}{\partial\hat{r}^2}+\frac{2}{\hat{r}}\frac{\partial\bar{\tilde{e}}}{\partial\hat{r}} - s\cdot\bar{\tilde{e}} = -\tilde{e}^o(\hat{r}), \quad \text{(A14)}$$

where $\tilde{e}^o(r)$ is the initial dilatation distribution (Eq. 28). Equation A14 can be integrated analytically with the method of variation of coefficients:

$$\bar{\tilde{e}}(\hat{r},s) = \frac{\tilde{p}_o}{(2\tilde{\mu}+\tilde{\lambda})(s-\tilde{\alpha}^2)}\left(1-\frac{\sinh(\tilde{\alpha}\hat{r})}{\hat{r}\sinh(\tilde{\alpha})}\right) + \frac{\tilde{\alpha}^2\tilde{p}_o}{(2\tilde{\mu}+\tilde{\lambda})s(s-\tilde{\alpha}^2)}\left(\frac{\sinh(\sqrt{s}\hat{r})}{\hat{r}\sinh(\sqrt{s})}-1\right). \quad \text{(A15)}$$

The expressions for IFP, velocity, and solid displacement can be obtained analogously to the previous case.

The final solutions in the time domain are

$$\tilde{e}(\hat{r},\hat{t}) = \frac{\tilde{p}_o}{(2\tilde{\mu}+\tilde{\lambda})}\left(1-\frac{\sinh(\tilde{\alpha}\hat{r})}{\hat{r}\sinh(\tilde{\alpha})}\right) + \frac{\tilde{\alpha}^2\tilde{p}_o}{(2\tilde{\mu}+\tilde{\lambda})}\frac{1}{\hat{r}}\sum_{n=1}^{\infty}\frac{2}{n\pi}(-1)^n c_n(1-e^{-n^2\pi^2\hat{t}}) \quad \text{(A16)}$$

$$\tilde{p}(\hat{r},\hat{t}) = \tilde{p}_o\left(1-\frac{\sinh(\tilde{\alpha}\hat{r})}{\hat{r}\sinh(\tilde{\alpha})}\right) + \frac{\tilde{\alpha}^2\tilde{p}_o}{\hat{r}}\sum_{n=1}^{\infty}\frac{2}{n\pi}(-1)^n c_n(1-e^{-n^2\pi^2\hat{t}}) \quad \text{(A17)}$$

$$\tilde{u}(\hat{r},\hat{t}) = \frac{R\tilde{p}_o}{(2\tilde{\mu}+\tilde{\lambda})}\left(\frac{\hat{r}}{3}-\frac{\tilde{\alpha}\hat{r}\cosh(\tilde{\alpha}\hat{r})-\sinh(\tilde{\alpha}\hat{r})}{\tilde{\alpha}^2\hat{r}^2\sinh(\tilde{\alpha})}\right) + \frac{R\tilde{\alpha}^2\tilde{p}_o}{(2\tilde{\mu}+\tilde{\lambda})}\frac{1}{\hat{r}^2}\sum_{n=1}^{\infty}\frac{2}{n\pi}(-1)^n\frac{c_n-n\pi\hat{r}d_n}{n^2\pi^2}(1-e^{-n^2\pi^2\hat{t}}) \quad \text{(A18)}$$

$$\hat{v}(\hat{r},\hat{t}) = \frac{\tilde{K}\tilde{p}_o}{R\tilde{\phi}}\left(\frac{\tilde{\alpha}\hat{r}\cosh(\tilde{\alpha}\hat{r})-\sinh(\tilde{\alpha}\hat{r})}{\hat{r}^2\sinh(\tilde{\alpha})}\right) + \frac{\tilde{K}\tilde{p}_o}{R\tilde{\phi}}\frac{\tilde{\alpha}^2}{\hat{r}^2}\sum_{n=1}^{\infty}\frac{2}{n\pi}(-1)^n(c_n-\hat{r}n\pi d_n)e^{-n^2\pi^2\hat{t}} + \frac{\tilde{K}\tilde{p}_o}{R\tilde{\phi}}\frac{\tilde{\alpha}^2}{\hat{r}^2}\sum_{n=1}^{\infty}\frac{2}{n\pi}(-1)^n\frac{c_n-n\pi\hat{r}d_n}{n\pi}(1-e^{-n^2\pi^2\hat{t}}). \quad \text{(A19)}$$

Manuscript received July 1, 1996, and revision received Nov. 4, 1996.